

# Network Massive MIMO Transmission Over Millimeter-Wave and Terahertz Bands: Mobility Enhancement and Blockage Mitigation

Li You, Xu Chen, Xiaohang Song, Fan Jiang, Wenjin Wang,  
Xiqi Gao, *Fellow, IEEE*, and Gerhard Fettweis, *Fellow, IEEE*

## Abstract

Mobility and blockage are two critical challenges in wireless transmission over millimeter-wave (mmWave) and Terahertz (THz) bands. In this paper, we investigate network massive multiple-input multiple-output (MIMO) transmission for mmWave/THz downlink in the presence of mobility and blockage. Considering the mmWave/THz propagation characteristics, we first propose to apply per-beam synchronization for network massive MIMO to mitigate the channel Doppler and delay dispersion effects. Accordingly, we establish a transmission model. We then investigate network massive MIMO downlink transmission strategies with only the statistical channel state information (CSI) available at the base stations (BSs), formulating the strategy design problem as an optimization problem to maximize the network sum-rate. We show that the beam domain is favorable to perform transmission, and demonstrate that BSs can work individually when sending signals to user terminals. Based on these insights, the network massive MIMO precoding design is reduced to a network sum-rate maximization problem with respect to beam domain power allocation. By exploiting the sequential optimization method and random matrix theory, an iterative algorithm with guaranteed convergence performance is further proposed for beam domain power allocation. Numerical results reveal that the proposed network massive MIMO

*Corresponding author: Xiqi Gao.*

This work will be presented in part at the IEEE International Conference on Communications, Dublin, Ireland, Jun. 2020 [1].

Li You, Xu Chen, Wenjin Wang, and Xiqi Gao are with the National Mobile Communications Research Laboratory, Southeast University, Nanjing 210096, China, and also with the Purple Mountain Laboratories, Nanjing 211100, China (e-mail: liyou@seu.edu.cn; chen\_xu@seu.edu.cn; wangwj@seu.edu.cn; xqgao@seu.edu.cn).

Xiaohang Song and Gerhard Fettweis are with the Vodafone Chair Mobile Communications Systems, Technische Universität Dresden, 01062 Dresden, Germany (e-mail: xiaohang.song@tu-dresden.de; gerhard.fettweis@tu-dresden.de).

Fan Jiang is with the Laboratory for Information and Decision Systems (LIDS), Massachusetts Institute of Technology (MIT), Cambridge, MA 02139 USA (e-mail: fjiang@mit.edu).

transmission approach with the statistical CSI can effectively alleviate the blockage effects and provide mobility enhancement over mmWave and THz bands.

### Index Terms

Millimeter-wave, Terahertz, per-beam synchronization, network massive MIMO, high mobility, blockage.

## I. INTRODUCTION

The shortage of global wireless spectrum resources at sub-6 GHz has prompted the exploration of millimeter-wave (mmWave) and Terahertz (THz) bands, where the spectrum is orders of magnitude higher than that in current cellular allocations [2]–[4]. Thanks to the deployment of large-scale antenna arrays at the base stations (BSs), massive multiple-input multiple-output (MIMO) could serve a plurality of user terminals (UTs) over the same time/frequency resources, remarkably increasing the system spectral efficiency [5]. From a practical point of view, combining mmWave/THz transmission with massive MIMO is a widespread concern [4], [6]–[12]. The short wavelength in mmWave/THz signals allows only a small physical space to encapsulate a large antenna array. Meanwhile, high beamforming gains of massive MIMO can solve the problem of high propagation path loss in mmWave/THz transmission.

Utilizing mmWave/THz frequencies for wireless communications has received significant attention over the past few years. Communicating over mmWave/THz bands is not merely a matter of adjusting the carrier frequency to the corresponding bands. The process is much more complicated. First, due to the short wavelength of mmWave/THz signals, the diffraction effects are negligible. Also, it is important to consider that, as the number of scattering clusters is relatively small, the propagation path loss over mmWave/THz bands exhibits different properties. In addition, mmWave/THz signals are highly sensitive to blockage due to high penetration loss [13], [14], which needs to be considered in transmission design. Furthermore, in high mobility scenarios, the Doppler spread for signal transmission over the mmWave/THz bands could be much larger, becoming a system implementation bottleneck to realize the promising vision of mmWave/THz communications [15].

Existing works in mmWave/THz communications have attempted to address these issues. Extensive measurement results for mmWave/THz channels have been reported in [16]–[21]. Detailed modeling methods for blockage effects and spatial propagation characteristics of the

mmWave channels have been studied in [22]. Based on the random shape theory, a statistic model was developed in [14] to quantify the blockage effects in mmWave propagation. To handle the mobility issue in MIMO transmissions, beam-based Doppler frequency synchronization for narrowband MIMO transmissions was suggested in [23]. For wideband massive MIMO wireless communications over mmWave/THz bands, a per-beam synchronization (PBS) approach was proposed in [9] motivated by the beam domain channel dispersion properties, where the synchronization is performed over each receive beam. In particular, the Doppler frequency spread with PBS can be approximately reduced by a factor of the number of UT antennas compared with the conventional synchronization approaches. In addition, assuming a fixed antenna array aperture, the number of antennas that can be accommodated scales linearly with the carrier frequency. Thus, the utilization of the PBS scheme can effectively alleviate the Doppler effect of the mmWave/THz transmission system [9].

Distinct from the existing multi-cell massive MIMO transmission in [24], [25], we investigate network massive MIMO transmission in this paper, allowing the BS to transmit signals to UTs in other cells<sup>1</sup> and the resultant diversity against the channel blockage over the mmWave/THz bands can be efficiently exploited. This can significantly alleviate the blockage effects while improving the transmission performance over mmWave/THz bands. However, network transmission will also pose emerging challenges, including the considerable overhead of information exchange between BSs and the increased complexity of transmission strategy design. We target these challenges in designing network massive MIMO transmission strategies in this paper.

The performance of network massive MIMO transmission is highly dependent on the accuracy of the obtained channel state information (CSI). Most previous works on multi-cell transmission designs [27]–[30] require the complete knowledge of the instantaneous CSI at the transmitter (CSIT). However, the acquisition of the instantaneous CSIT is usually challenging in massive MIMO downlink (DL), especially over the mmWave/THz bands. For instance, utilizing the uplink (UL) and DL channel reciprocity, DL CSI can be obtained via UL channel estimation in time-division duplex systems. However, the obtained DL CSI can be inaccurate due to, e.g., the calibration error of the radio frequency chains [31]. Even worse, in frequency-division duplex systems without channel reciprocity, the CSI feedback overhead scales with the number of transmit antennas when orthogonal pilot sequences are adopted. The huge amount overhead is

<sup>1</sup>Network massive MIMO systems are different from cell-free massive MIMO systems where the access points and UTs are all equipped with only one antenna [26].

unacceptable in practical mmWave/THz network massive MIMO systems. Moreover, when the UTs are in high mobility [32], the channel fluctuation behaves much severer, and the acquired CSI quickly becomes outdated. Compared with the instantaneous CSI, the statistical CSI, e.g., the spatial correlation and channel mean, varies more slowly and can be easily and accurately obtained by the BSs through, e.g., long-term feedback or covariance extrapolation [33], [34]. Therefore, the statistical CSI can be exploited for wireless transmission designs [9], [25], [35], [36], especially in the considered mmWave/THz network massive MIMO transmission system.

Motivated by the above considerations, we investigate the network massive MIMO transmission strategy design for mmWave/THz systems with the availability of the statistical CSIT at the BSs. The major contributions of this paper are summarized as follows

- We establish the network massive MIMO channel model over mmWave/THz bands, and propose a PBS scheme in both time and frequency dimensions to mitigate the channel Doppler and delay dispersion. The utilization of the PBS scheme makes the transmission design over mmWave/THz bands nearly the same as that over the regular bands; as a result, even in high mobility scenarios, the problem formulation and the corresponding analysis of the mmWave/THz transmission can be simplified.
- We formulate the problem to design the optimal DL transmission strategy as the maximization of the network sum-rate based on the PBS scheme. We then derive the necessary condition of the optimal transmit covariance matrices. The necessary condition reveals that with a sufficiently large number of transmit antennas, the beam domain is favorable to the DL transmission and the individual signals to the UTs from multiple BSs are possible.
- We explore a novel low-complexity algorithm to solve the above formulated problem. This is done by transforming the original precoder design problem into a beam domain power allocation problem. We show that the new problem is a concave-convex problem, and it can be efficiently solved by exploiting the concave-convex procedure (CCCP). We further derive a deterministic equivalent (DE) of the optimization objective, which can be calculated in low complexity.
- We demonstrate the efficiency of the proposed low-complexity algorithm through the exploitation of the Karush-Kuhn-Tucker (KKT) conditions and numerical simulations. Specifically, we show that the solution of each CCCP iteration has a structure similar to the classical water-filling solution. Based on that, we further develop an iterative water-filling power allocation algorithm with guaranteed convergence performance. Extensive numerical

simulations are also conducted and the results strongly validate the significant performance improvement of the proposed network massive MIMO transmission approach over existing approaches in mmWave/THz bands, especially in highly mobile scenarios.

The rest of this paper is organized as follows. In Section II, we establish the mmWave/THz massive MIMO channel model with blockage effects and the transmission signal model after PBS. We then investigate the network transmission strategy to maximize the network DL transmission sum-rate with the statistical CSIT only in Section III. Extensive numerical results are presented in Section IV. Finally, the conclusions are drawn in Section V.

We adopt the following notations throughout the paper. Upper-case and lower-case boldface letters indicate matrices and column vectors, respectively. We adopt  $\bar{j} = \sqrt{-1}$  to denote the imaginary unit. We use  $\mathbf{I}_N$  to denote the  $N \times N$  identity matrix. The superscripts  $(\cdot)^T$ ,  $(\cdot)^{-1}$ , and  $(\cdot)^H$  represent the matrix transpose, inverse, and conjugate-transpose operations, respectively. The ensemble expectation, matrix trace, and determinant operations are represented by  $\mathbb{E}\{\cdot\}$ ,  $\text{tr}(\cdot)$ , and  $\det(\cdot)$ , respectively.  $\mathcal{N}(a, \xi^2)$  represents the real-valued Gaussian distribution with mean  $a$  and covariance  $\xi^2$ . We use  $[\mathbf{A}]_{m,n}$ ,  $[\mathbf{A}]_{i,:}$ ,  $[\mathbf{A}]_{:,j}$  and  $[\mathbf{a}]_m$  to represent the  $(m, n)$ -th element, the  $i$ -th row, the  $j$ -th column of matrix  $\mathbf{A}$ , and the  $m$ -th element of column vector  $\mathbf{a}$ , respectively. The operator  $\text{diag}\{\mathbf{x}\}$  is to form a diagonal matrix with its  $m$ -th diagonal element being  $[\mathbf{x}]_m$ .  $\lfloor x \rfloor$  is the floor function to obtain the largest integer not greater than  $x$ . The operator  $\langle \cdot \rangle_M$  denotes the modulo- $M$  operation.  $\delta(\cdot)$  denotes the Dirac's delta function. The inequality  $\mathbf{A} \succeq \mathbf{0}$  means that  $\mathbf{A}$  is a Hermitian positive semi-definite matrix. The notation  $[x]^+$  denotes  $\max(x, 0)$ . The symbols  $\odot$  and  $\otimes$  are reserved for the Hadamard and Kronecker products, respectively. The notation  $\triangleq$  is used for definitions.

## II. SYSTEM MODEL

### A. System Setup

We consider a network massive MIMO DL cellular system consisting of  $U$  cells, where each cell  $u \in \mathcal{U} \triangleq \{1, \dots, U\}$  contains one  $M_u$ -antennas BS and  $K_u$  multi-antenna UTs.<sup>2</sup> Denote the BS in cell  $u$  and the  $k$ -th UT in cell  $u$  as BS- $u$  and UT- $(k, u)$ , respectively. The set of all UTs is denoted by  $\mathcal{K} \triangleq \{(k, u) | k = 1 \dots, K_u; u = 1, \dots, U\}$ . Note that there is a central processor in the considered network DL transmission, and BS- $u \in \mathcal{U}$  can send signals to all UTs- $(k, u) \in \mathcal{K}$ .

<sup>2</sup> Note that  $U$  is finite in practical systems, due to the implementation complexity considerations. In our work, we assume that the signals sent by the BSs outside the network contribute to the effective noise [37].

Assume that BS- $u$  is equipped with a uniform planar array (UPA) consisting of  $M_u = M_u^h \times M_u^v$  antennas, where half-wavelength spacing is used in both horizontal and vertical directions. The numbers of antennas in horizontal and vertical directions are  $M_u^h$  and  $M_u^v$ , respectively. The number of total BS antennas in the system is  $M_{\text{tot}} = \sum_{u=1}^U M_u$ .<sup>3</sup> In addition, each UT- $(k, u)$  is equipped with a uniform linear array (ULA) consisting of  $N_{k,u}$  antennas with half-wavelength antenna spacing.

Orthogonal frequency division multiplexing (OFDM) modulation is adopted with  $N_{\text{us}}$  sub-carriers, appended with the cyclic prefix (CP) of length  $N_{\text{cp}}$ . The OFDM symbol duration and CP duration are  $T_{\text{us}} = N_{\text{us}} \times T_s$  and  $T_{\text{cp}} = N_{\text{cp}} \times T_s$ , respectively, where  $T_s$  is the system sampling interval.

### B. Channel Model

A three-state statistical model is adopted to describe the mmWave/THz massive MIMO channel states, where each propagation link can be in one of three states: line-of-sight (LOS), non line-of-sight (NLOS), and outage states.<sup>4</sup> The corresponding probability functions of the channels between BS- $v$  and UT- $(k, u)$  in each state can be written as

$$p_{\text{out}}(d_{k,u,v}) = \max(0, 1 - e^{-a_{\text{out}}d_{k,u,v} + b_{\text{out}}}), \quad (1a)$$

$$p_{\text{LOS}}(d_{k,u,v}) = (1 - p_{\text{out}}(d_{k,u,v})) e^{-a_{\text{los}}d_{k,u,v}}, \quad (1b)$$

$$p_{\text{NLOS}}(d_{k,u,v}) = 1 - p_{\text{out}}(d_{k,u,v}) - p_{\text{LOS}}(d_{k,u,v}), \quad (1c)$$

respectively, where  $d_{k,u,v}$  is the distance between the BS and the UT, and  $a_{\text{out}}$ ,  $a_{\text{los}}$ , and  $b_{\text{out}}$  are parameters that fit from the data [22]. According to the channel measurement campaigns [22], [29], the large-scale path loss from BS- $v$  to UT- $(k, u)$  in a given state can be modeled via a standard linear form as

$$\zeta_{k,u,v}^{\text{sta}}(d_{k,u,v}) [\text{in dB}] = a^{\text{sta}} + b^{\text{sta}} 10 \log_{10}(d_{k,u,v}) + c^{\text{sta}}, \quad (2)$$

<sup>3</sup> The BSs in the network act as a single distributed multi-antenna transmitter with  $M_{\text{tot}}$  antennas, perfectly coordinated by a central controller, serving all UTs in the network [37].

<sup>4</sup> Compared with the channel model over the regular bands where each link is in either a LOS or NLOS state, the adopted three-state model incorporates an additional outage state which can describe the channel blockage effect over the mmWave and THz bands [22], [38].

where the superscript  $\text{sta} \in \{\text{LOS}, \text{NLOS}, \text{out}\}$  represents the state of the link,  $\mathbf{a}^{\text{sta}}$ ,  $\mathbf{b}^{\text{sta}}$ , and  $c^{\text{sta}}$  are parameters that fit from the measurement results. In addition,  $c^{\text{sta}} \in \mathcal{N}(0, (\xi^{\text{sta}})^2)$  where  $(\xi^{\text{sta}})^2$  describes the shadowing variance. Note that these propagation state related parameters which represent large-scale fading vary relatively slowly compared to the instantaneous CSI. In the following, we model the channel parameters for a specific state where the propagation state index is omitted for notational brevity.

According to the adopted configurations of the BS and UT antennas, steering vectors of UT- $(k, u)$  and BS- $v$  corresponding to the angles of arrival/departure (AoA/AoD) are given by

$$\mathbf{a}_{\text{ut},k,u}(\theta) = [1, e^{-j\pi\theta}, \dots, e^{-j\pi(N_{k,u}-1)\theta}]^T \in \mathbb{C}^{N_{k,u} \times 1}, \quad (3a)$$

$$\mathbf{a}_{\text{bs},v}(\alpha, \beta) = [1, e^{-j\pi\alpha}, \dots, e^{-j\pi(M_v^h-1)\alpha}]^T \otimes [1, e^{-j\pi\beta}, \dots, e^{-j\pi(M_v^v-1)\beta}]^T \in \mathbb{C}^{M_v \times 1}, \quad (3b)$$

respectively, where  $\theta$  is an auxiliary angle related to AoA  $\vartheta \in [-\pi/2, \pi/2]$  as  $\theta = \sin \vartheta \in [-1, 1]$ .  $\alpha$  and  $\beta$  are auxiliary angles related to elevation AoD  $\phi_1 \in [-\pi/2, \pi/2]$  and azimuth AoD  $\phi_2 \in [-\pi/2, \pi/2]$  as  $\alpha = \cos \phi_2 \sin \phi_1 \in [-1, 1]$  and  $\beta = \sin \phi_2 \sin \phi_1 \in [-1, 1]$ , respectively.<sup>5</sup> Then, the baseband space domain channel response matrix from BS- $v$  to UT- $(k, u)$  at time  $t$  and frequency  $f$  at a specific propagation state can be modeled as [9], [22], [29]

$$\mathbf{H}_{k,u,v}(t, f) = \int_{-1}^1 \int_{-1}^1 \int_{-1}^1 \underbrace{\sqrt{\frac{M_v N_{k,u}}{\zeta_{k,u,v}(d_{k,u,v}) \eta_{k,u,v}} \varphi_{k,u,v}(\theta, \alpha, \beta)}}_{\triangleq \sqrt{S_{k,u,v}(\theta, \alpha, \beta)}} \cdot e^{j\psi(\theta, \alpha, \beta)} \cdot e^{j2\pi[t\nu_{k,u,v}(\theta) - f\tau_{k,u,v}(\theta, \alpha, \beta)]} \cdot \mathbf{a}_{\text{ut},k,u}(\theta) \mathbf{a}_{\text{bs},v}^H(\alpha, \beta) d\alpha d\beta d\theta \in \mathbb{C}^{N_{k,u} \times M_v}, \quad (4)$$

where  $\eta_{k,u,v}$  is the number of channel paths between BS- $v$  and UT- $(k, u)$ .  $\psi(\theta, \alpha, \beta)$  is a random phase uniformly distributed in  $[0, 2\pi)$ .  $\nu_{k,u,v}(\theta)$  is the Doppler shift associated with  $\theta$  and linear over the carrier frequency [9].  $\tau_{k,u,v}(\theta, \alpha, \beta)$  is the path delay associated with auxiliary AoA-AoD pair  $(\theta, \alpha, \beta)$ , and  $\varphi_{k,u,v}(\theta, \alpha, \beta)$  is the normalized average power of the channel path associated with auxiliary AoA-AoD pair  $(\theta, \alpha, \beta)$  from BS- $v$  to UT- $(k, u)$ . Note that for a specific propagation state, the large-scale path loss  $\zeta_{k,u,v}(d_{k,u,v})$  can be modeled using (2).

Based on (4), we define the DL beam domain channel response matrix from BS- $v$  to UT- $(k, u)$

<sup>5</sup>Note that the array response vectors,  $\mathbf{a}_{\text{ut},k,u}(\theta)$  and  $\mathbf{a}_{\text{bs},v}(\alpha, \beta)$ , can usually be assumed to be not related to the actual operating frequency in practical wideband mmWave/THz wireless systems as the bandwidth is usually much smaller compared with the carrier frequency [10].

at time  $t$  and frequency  $f$  as [9], [39]

$$\tilde{\mathbf{H}}_{k,u,v}(t, f) \triangleq \mathbf{V}_{N_{k,u}}^H \mathbf{H}_{k,u,v}(t, f) (\mathbf{V}_{M_v^h} \otimes \mathbf{V}_{M_v^v}) \in \mathbb{C}^{N_{k,u} \times M_v}, \quad (5)$$

where  $\mathbf{V}_N \in \mathbb{C}^{N \times N}$  is the unitary discrete Fourier transform (DFT) matrix. Note that the channel model in (5) can also be applied to systems with lens antenna array [40]. For mmWave/THz massive MIMO channels where  $N_{k,u}$ ,  $M_v^h$  and  $M_v^v$  are all sufficiently large, the beam domain channel matrix elements in (5) can be well approximated by [9]

$$\begin{aligned} \left[ \tilde{\mathbf{H}}_{k,u,v}(t, f) \right]_{i,j} &\approx \int_{\alpha_{m_j}}^{\alpha_{m_j+1}} \int_{\beta_{n_j}}^{\beta_{n_j+1}} \int_{\theta_i}^{\theta_i+1} \sqrt{S_{k,u,v}(\theta, \alpha, \beta)} \cdot e^{\bar{j}\psi(\theta, \alpha, \beta)} \\ &\cdot e^{\bar{j}2\pi[t\nu_{k,u,v}(\theta) - f\tau_{k,u,v}(\theta, \alpha, \beta)]} d\alpha d\beta d\theta, \end{aligned} \quad (6)$$

where  $m_j \triangleq \langle j \rangle_{M_v^h}$ ,  $n_j \triangleq \lfloor j/M_v^h \rfloor$ ,  $\alpha_{m_j} \triangleq 2m_j/M_v^h - 1$ ,  $\beta_{n_j} \triangleq 2n_j/M_v^v - 1$ , and  $\theta_i \triangleq 2i/N_{k,u} - 1$ . As a result, the DL beam domain channel impulse response matrix from BS- $v$  to UT- $(k, u)$  at time  $t$  and delay  $\tau$  can be obtained as

$$\begin{aligned} \left[ \tilde{\mathbf{H}}_{k,u,v}(t, \tau) \right]_{i,j} &= \int_{\alpha_{m_j}}^{\alpha_{m_j+1}} \int_{\beta_{n_j}}^{\beta_{n_j+1}} \int_{\theta_i}^{\theta_i+1} \sqrt{S_{k,u,v}(\theta, \alpha, \beta)} \cdot e^{\bar{j}\psi(\theta, \alpha, \beta)} \\ &\cdot e^{\bar{j}2\pi t\nu_{k,u,v}(\theta)} \cdot \delta(\tau - \tau_{k,u,v}(\theta, \alpha, \beta)) d\alpha d\beta d\theta, \end{aligned} \quad (7)$$

which is the inverse Fourier transform of  $\tilde{\mathbf{H}}_{k,u,v}(t, f)$  with respect to  $f$ . Note that the Doppler and delay spreads of the DL channels over a specific receive beam will be much smaller compared with those of the space domain channels due to the directional properties of the mmWave/THz channels [9]. In the following, we will adopt (7) to simplify the analysis.

### C. Transmission Model

We consider the beam domain transmission for massive MIMO transmission over the mmWave and THz bands. After OFDM modulation, the DL transmitted signal of BS- $v$  in the given OFDM block,  $\mathbf{x}_v(t) \in \mathbb{C}^{M_v \times 1}$ , can be represented as [41]

$$\mathbf{x}_v(t) = \sum_{s=0}^{N_{\text{us}}-1} \mathbf{x}_{v,s} \cdot e^{\bar{j}2\pi \frac{s}{T_{\text{us}}} t}, \quad -T_{\text{cp}} \leq t < T_{\text{us}}, \quad (8)$$

where  $\mathbf{x}_{v,s} = \sum_{\forall(k,u)} \mathbf{x}_{k,u,v,s}$  is the beam domain signal transmitted from BS- $v$  at the  $s$ -th sub-carrier, and  $\mathbf{x}_{k,u,v,s}$  is the signal from BS- $v$  to UT- $(k,u)$  at sub-carrier  $s$ . Here, we omit the OFDM transmission block index for convenience. Accordingly, the received beam domain signal by UT- $(k,u)$  at time  $t$  can be expressed as

$$\mathbf{y}_{k,u}(t) = \sum_{v=1}^U \int_{-\infty}^{\infty} \tilde{\mathbf{H}}_{k,u,v}(t, \tau) \mathbf{x}_v(t - \tau) d\tau \in \mathbb{C}^{N_{k,u} \times 1}, \quad (9)$$

where  $\tilde{\mathbf{H}}_{k,u,v}(t, \tau)$  is defined in (7). Note that possible inter-block interference (IBI) and noise are ignored in the transmission model (9) for clarity.

The received signal  $\mathbf{y}_{k,u}(t)$  suffers from time offsets  $\tau_{k,u} \in [\tau_{k,u}^{\min}, \tau_{k,u}^{\max}]$ , and Doppler offsets  $\nu_{k,u} \in [\nu_{k,u}^{\min}, \nu_{k,u}^{\max}]$ , which severely affect the transmission performance. To mitigate these effects, we perform time and frequency compensation at the UT receiver. Different from the traditional space domain synchronization method [42], we propose to apply the PBS scheme [9] in our network transmission framework.

Due to the highly directional propagation properties of the mmWave/THz signals, the received signal of a specific UT- $(k,u)$  on a particular receive beam will exhibit smaller delay and Doppler spreads compared with the space domain signals [9], [40]. In other words, the  $i$ -th element of the beam domain received signal  $\mathbf{y}_{k,u}(t)$ , i.e.,  $y_{k,u,i}(t)$ , will experience the time offsets ranging from  $\tau_{k,u,i}^{\min}$  to  $\tau_{k,u,i}^{\max}$  as well as the frequency offsets ranging from  $\nu_{k,u,i}^{\min}$  to  $\nu_{k,u,i}^{\max}$ . We then perform the PBS scheme, i.e., to apply time and frequency adjustment parameters as  $\tau_{k,u,i}^{\text{syn}} = \tau_{k,u,i}^{\min}$  and  $\nu_{k,u,i}^{\text{syn}} = (\nu_{k,u,i}^{\max} + \nu_{k,u,i}^{\min})/2$  [9]. As a result, the received signal over beam  $i$  of UT- $(k,u)$  is given by

$$y_{k,u,i}^{\text{pbs}}(t) = y_{k,u,i}(t + \tau_{k,u,i}^{\text{syn}}) \cdot e^{-j2\pi(t + \tau_{k,u,i}^{\text{syn}})\nu_{k,u,i}^{\text{syn}}}. \quad (10)$$

Then, the received signals over all beams after PBS can be represented as

$$\mathbf{y}_{k,u}^{\text{pbs}}(t) = \left[ y_{k,u,0}^{\text{pbs}}(t), y_{k,u,1}^{\text{pbs}}(t), \dots, y_{k,u,N_{k,u}-1}^{\text{pbs}}(t) \right]^T. \quad (11)$$

After CP removal and DFT operation, the demodulated OFDM symbol over beam  $i$  of UT- $(k,u)$  at sub-carrier  $s$  is [9], [41]

$$y_{k,u,i,s} = \frac{1}{T_{\text{us}}} \int_0^{T_{\text{us}}} y_{k,u,i}^{\text{pbs}}(t) \cdot e^{-j2\pi \frac{s}{T_{\text{us}}} t} dt$$

$$= \sum_{v=1}^U \sum_{j=0}^{M_v-1} [\mathbf{G}_{k,u,v,s}]_{i,j} [\mathbf{x}_{v,s}]_j, \quad (12)$$

where  $\mathbf{G}_{k,u,v,s} \in \mathbb{C}^{N_{k,u} \times M_v}$  denotes the equivalent beam domain channel from BS- $v$  to UT- $(k, u)$  after PBS at sub-carrier  $s$  in the given block. Its  $(i, j)$ -th element is given by [9]

$$[\mathbf{G}_{k,u,v,s}]_{i,j} \triangleq \int_{\alpha_{m_j}}^{\alpha_{m_j+1}} \int_{\beta_{n_j}}^{\beta_{n_j+1}} \int_{\theta_i}^{\theta_{i+1}} \sqrt{S_{k,u,v}(\theta, \alpha, \beta)} \cdot e^{\bar{j}\psi(\theta, \alpha, \beta)} \cdot e^{-\bar{j}2\pi \frac{s}{T_{\text{us}}}} (\tau_{k,u,v}(\theta, \alpha, \beta) - \tau_{k,u,i}^{\text{syn}}) \cdot e^{\bar{j}2\pi \tau_{k,u,i}^{\text{syn}} (\nu_{k,u,v}(\theta) - \nu_{k,u,i}^{\text{syn}})} d\alpha d\beta d\theta. \quad (13)$$

*Remark 1:* In practical OFDM systems, the values of  $T_{\text{cp}}$  and  $T_{\text{us}}$  should satisfy the following condition [41]

$$\max_{k,u} \{ \Delta_{\tau_{k,u}} \} \leq T_{\text{cp}} \leq T_{\text{us}} \ll 1 / \max_{k,u} \{ \Delta_{\nu_{k,u}} \}, \quad (14)$$

where  $\Delta_{\tau_{k,u}}$  and  $\Delta_{\nu_{k,u}}$  are the effective channel delay and frequency spreads after synchronization, respectively. Note that in the traditional space domain synchronization method, the corresponding effective channel delay and Doppler frequency spreads are given by  $\Delta_{\tau_{k,u}}^{\text{spa}} = \tau_{k,u}^{\text{max}} - \tau_{k,u}^{\text{min}}$ , and  $\Delta_{\nu_{k,u}}^{\text{spa}} = (\nu_{k,u}^{\text{max}} - \nu_{k,u}^{\text{min}}) / 2$ , respectively [43]. As  $\Delta_{\nu_{k,u}}^{\text{spa}}$  is linear with the velocity and the carrier frequency [9], it is difficult to select proper OFDM parameters for mmWave/THz transmission in high mobility scenarios. However, with the application of the PBS scheme, the effective delay spread,  $\Delta_{\tau_{k,u}}^{\text{per}} = \max_i \{ \tau_{k,u,i}^{\text{max}} - \tau_{k,u,i}^{\text{min}} \} \leq \Delta_{\tau_{k,u}}^{\text{spa}}$ , and the effective Doppler frequency spread,  $\Delta_{\nu_{k,u}}^{\text{per}} = \max_i \left\{ \frac{\nu_{k,u,i}^{\text{max}} - \nu_{k,u,i}^{\text{min}}}{2} \right\} = \Delta_{\nu_{k,u}}^{\text{spa}} / N_{k,u}$ , can be significantly reduced [9]. More importantly, the PBS makes the transmission design over mmWave/THz bands approximately the same as that over the regular bands, which can effectively mitigate the mobility issue in mmWave/THz transmission.

With the PBS scheme applied, we can obtain the network massive MIMO-OFDM beam domain transmission model over each subcarrier given by

$$\mathbf{y}_{k,u,s} = \sum_{v=1}^U \mathbf{G}_{k,u,v,s} \mathbf{x}_{v,s} \in \mathbb{C}^{N_{k,u} \times 1}, \quad s = 0, 1, \dots, N_{\text{us}} - 1. \quad (15)$$

It should be noted that if the traditional synchronization method is adopted, a more complicated transmission model involving, e.g., inter-carrier interference (ICI), should be considered. This will lead to complexity in the transmission design [9], [41]. From (13), the elements of the

equivalent channel after PBS,  $\mathbf{G}_{k,u,v,s}$ , are uncorrelated, and the corresponding statistical CSI can be modeled as [9]

$$\mathbf{\Omega}_{k,u,v,s} = \mathbb{E} \left\{ \mathbf{G}_{k,u,v,s} \odot \mathbf{G}_{k,u,v,s}^* \right\}, \quad (16)$$

where the element  $[\mathbf{\Omega}_{k,u,v,s}]_{i,j}$  corresponds to the average power of  $[\mathbf{G}_{k,u,v,s}]_{i,j}$ , capturing the average coupling effect between the  $j$ -th transmit eigenmode of BS- $v$  and the  $i$ -th receive eigenmode of UT- $(k, u)$  as

$$[\mathbf{\Omega}_{k,u,v,s}]_{i,j} = \int_{\alpha_{m_j}}^{\alpha_{m_j+1}} \int_{\beta_{n_j}}^{\beta_{n_j+1}} \int_{\theta_i}^{\theta_{i+1}} S_{k,u,v}(\theta, \alpha, \beta) d\alpha d\beta d\theta. \quad (17)$$

Note that the statistical CSI,  $\mathbf{\Omega}_{k,u,v,s}$ , is independent of sub-carriers; as a result, the sub-carrier subscript  $s$  in (17) can be omitted, i.e.,  $\mathbf{\Omega}_{k,u,v,s} = \mathbf{\Omega}_{k,u,v}, \forall s$ . Therefore, the transmission strategies utilizing the statistical CSI are identical over all subcarriers. This can significantly reduce the overhead of the CSI acquisition at the transmitter and the complexity in practical wideband transmission strategy design.

### III. NETWORK DOWNLINK TRANSMISSION

In this section, we investigate DL transmission with PBS for mmWave/THz network massive MIMO systems. Note that if PBS is not performed as described in Section II, it is difficult to select proper OFDM parameters, especially in high mobility scenarios. Also, the ICI as well as IBI should be properly handled. Therefore, we design the network DL transmission strategy in this section based on the PBS scheme and the transmission model in (15).

In our DL network transmission strategy design, we assume that only the statistical CSI of UTs in the network is available at the transmitter, e.g.,  $\mathbf{\Omega}_{k,u,v}$ . Based on (15), a compact beam domain representation of the network transmission over the mmWave/THz bands can be written as

$$\begin{aligned} \mathbf{y}_{k,u} &= \sum_{v=1}^U \mathbf{G}_{k,u,v} \mathbf{x}_v + \mathbf{n}_{k,u} \\ &= \sum_{v=1}^U \mathbf{G}_{k,u,v} \mathbf{x}_{k,u,v} + \sum_{v=1}^U \sum_{(i,j) \neq (k,u)} \mathbf{G}_{k,u,v} \mathbf{x}_{i,j,v} + \mathbf{n}_{k,u} \\ &= \mathbf{G}_{k,u} \mathbf{x}_{k,u} + \sum_{(i,j) \neq (k,u)} \mathbf{G}_{k,u} \mathbf{x}_{i,j} + \mathbf{n}_{k,u} \in \mathbb{C}^{N_{k,u} \times 1}, \end{aligned} \quad (18)$$

where  $\mathbf{x}_{k,u,v}$  is the signal for UT- $(k, u)$  transmitted from BS- $v$  in the beam domain,  $\mathbf{G}_{k,u} = [\mathbf{G}_{k,u,1}, \mathbf{G}_{k,u,2}, \dots, \mathbf{G}_{k,u,U}] \in \mathbb{C}^{N_{k,u} \times M_{\text{tot}}}$ ,  $\mathbf{x}_{k,u} = [\mathbf{x}_{k,u,1}^T, \dots, \mathbf{x}_{k,u,U}^T]^T \in \mathbb{C}^{M_{\text{tot}} \times 1}$ , and the indices of the OFDM symbols and the subcarriers are omitted for brevity. The transmitted signal  $\mathbf{x}_{k,u}$  satisfies  $\mathbb{E}\{\mathbf{x}_{k,u}\} = \mathbf{0}, \forall (k, u)$ , and  $\mathbb{E}\{\mathbf{x}_{k,u}\mathbf{x}_{i,j}^H\} = \mathbf{0}, \forall (i, j) \neq (k, u)$ . The covariance matrix of  $\mathbf{x}_{k,u}$  is  $\mathbf{Q}_{k,u} = \mathbb{E}\{\mathbf{x}_{k,u}\mathbf{x}_{k,u}^H\} \in \mathbb{C}^{M_{\text{tot}} \times M_{\text{tot}}}$ . The noise  $\mathbf{n}_{k,u} \in \mathbb{C}^{N_{k,u} \times 1}$  is circularly symmetric complex-valued Gaussian distributed with mean  $\mathbf{0}$  and covariance matrix  $\sigma^2 \mathbf{I}_{N_{k,u}}$ .

Denote by  $\mathbf{z}_{k,u} \triangleq \sum_{(i,j) \neq (k,u)} \mathbf{G}_{k,u} \mathbf{x}_{i,j} + \mathbf{n}_{k,u}$  the aggregate noise-plus-interference (NPI) component at UT- $(k, u)$ . With the properly designed DL pilots, each UT- $(k, u)$  is able to obtain its instantaneous CSI [9], [44]. Using a worst-case transmission design [45], and assuming the NPI component to be an equivalent Gaussian noise vector, we then have the corresponding covariance matrix  $\mathbf{K}_{k,u} = \mathbb{E}\{\mathbf{z}_{k,u}\mathbf{z}_{k,u}^H\}$  given by

$$\mathbf{K}_{k,u} = \sigma^2 \mathbf{I}_{N_{k,u}} + \sum_{(i,j) \neq (k,u)} \underbrace{\mathbb{E}\{\mathbf{G}_{k,u} \mathbf{Q}_{i,j} \mathbf{G}_{k,u}^H\}}_{\triangleq \mathbf{\Xi}_{k,u}(\mathbf{Q}_{i,j})}. \quad (19)$$

Note that  $\mathbf{\Xi}_{k,u}(\mathbf{X})$  defined in (19) is a matrix-valued function of  $\mathbf{X}$ . Using the independently distributed properties of the beam domain channel  $\mathbf{G}_{k,u}$ , we can obtain that  $\mathbf{\Xi}_{k,u}(\mathbf{X})$  is a diagonal matrix with the  $n$ -th element given by

$$[\mathbf{\Xi}_{k,u}(\mathbf{X})]_{n,n} = \text{tr} \left( \text{diag} \left\{ \left( [\boldsymbol{\Omega}_{k,u}]_{n,:} \right)^T \right\} \mathbf{X} \right), \quad (20)$$

where  $\boldsymbol{\Omega}_{k,u} = \mathbb{E}\{\mathbf{G}_{k,u} \odot \mathbf{G}_{k,u}^*\}$  is the beam domain statistical CSI. As a result, the DL ergodic transmission rate of UT- $(k, u)$  is obtained as [46]

$$R_{k,u} = \mathbb{E} \left\{ \log \left( \det \left( \mathbf{K}_{k,u} + \mathbf{G}_{k,u} \mathbf{Q}_{k,u} \mathbf{G}_{k,u}^H \right) \right) \right\} - \log \left( \det \left( \mathbf{K}_{k,u} \right) \right). \quad (21)$$

Eq. (21) indicates that the rate is a function of  $\mathbf{Q}_{k,u}, \forall (k, u)$ . Alternatively, we are able to design the network transmission strategy with the statistical CSIT to maximize the network sum-rate under the given constraints. Specifically, our design objective is to identify the optimal transmit covariance matrices under a per BS power constraint, which can be formulated as<sup>6</sup>

$$\arg \max_{\{\mathbf{Q}_{k,u}, \forall (k,u)\}} R = \sum_{u=1}^U \sum_{k=1}^{K_u} R_{k,u}$$

<sup>6</sup>Notice that the network transmission design can also be formulated using the weighted sum rate maximization criterion with UTs' quality-of-service requirements taken into account.

$$\begin{aligned}
\text{s.t.} \quad & \text{tr} \left( \sum_{u=1}^U \sum_{k=1}^{K_u} \mathbf{E}_v \mathbf{Q}_{k,u} \right) \leq P_v, & \forall v \in \mathcal{U}, \\
& \mathbf{Q}_{k,u} \succeq \mathbf{0}, & \forall (k, u) \in \mathcal{K},
\end{aligned} \tag{22}$$

where  $\mathbf{E}_v = \text{diag} \left\{ \mathbf{0}_{1 \times \sum_{v'=1}^{v-1} M_{v'}}, \mathbf{1}_{1 \times M_v}, \mathbf{0}_{1 \times \sum_{v'=v+1}^U M_{v'}} \right\}$ , and  $P_v$  denotes the power budget of BS- $v$ .

### A. Optimality of Beam Domain Transmission

We denote the eigenvalue decomposition of the beam domain transmit covariance matrix as  $\mathbf{Q}_{k,u} = \mathbf{U}_{k,u} \mathbf{\Lambda}_{k,u} \mathbf{U}_{k,u}^H$ .  $\mathbf{U}_{k,u}$  represents the subspace in which the transmitted signals from all BSs to UT- $(k, u)$  fall, and the elements of the diagonal matrix  $\mathbf{\Lambda}_{k,u}$  represent the power allocated to each direction of the subspace for the transmit signals. The following theorem identifies the optimal eigenmatrix  $\mathbf{U}_{k,u}, \forall (k, u)$ .

*Theorem 1:* For problem (22), the eigenmatrix,  $\mathbf{U}_{k,u}, \forall (k, u)$ , of the optimal transmit covariance matrix,  $\mathbf{Q}_{k,u}, \forall (k, u)$ , exhibits the following structure

$$\mathbf{U}_{k,u} = \mathbf{I}_{M_{\text{tot}}}, \quad \forall (k, u). \tag{23}$$

*Proof:* Please refer to Appendix A. ■

Theorem 1 reveals that to maximize the DL network sum-rate  $R$ , the signal transmission can be performed in the beam domain. In addition, according to Theorem 1,  $\mathbb{E}\{\mathbf{x}_{k,u,v} \mathbf{x}_{k,u,v'}^H\} = \mathbf{0}$  ( $\forall v \neq v'$ ), implying that it is not necessary to jointly design the signals sent by different BSs. In other words, different BSs can work individually when sending signals to a specific UT.

Based on Theorem 1, the optimization of the transmit covariance matrices in (22) can be simplified as the following beam domain power allocation problem, given by

$$\begin{aligned}
& \arg \max_{\mathbf{\Lambda} \triangleq \{\mathbf{\Lambda}_{k,u}, \forall (k,u)\}} \sum_{u=1}^U \sum_{k=1}^{K_u} (f_{k,u}^+(\mathbf{\Lambda}) - f_{k,u}^-(\mathbf{\Lambda})) \\
\text{s.t.} \quad & \text{tr} \left( \sum_{u=1}^U \sum_{k=1}^{K_u} \mathbf{E}_v \mathbf{\Lambda}_{k,u} \right) \leq P_v, \quad \forall v \in \mathcal{U}, \\
& \mathbf{\Lambda}_{k,u} \succeq \mathbf{0}, \quad \mathbf{\Lambda}_{k,u} \text{ diagonal}, \quad \forall (k, u) \in \mathcal{K},
\end{aligned} \tag{24}$$

where

$$f_{k,u}^+(\mathbf{\Lambda}) \triangleq \mathbb{E} \left\{ \log \left( \det \left( \mathbf{K}_{k,u}(\mathbf{\Lambda}) + \mathbf{G}_{k,u} \mathbf{\Lambda}_{k,u} \mathbf{G}_{k,u}^H \right) \right) \right\}, \quad (25)$$

$$f_{k,u}^-(\mathbf{\Lambda}) \triangleq \log \left( \det \left( \mathbf{K}_{k,u}(\mathbf{\Lambda}) \right) \right), \quad (26)$$

$$\mathbf{K}_{k,u}(\mathbf{\Lambda}) \triangleq \sigma^2 \mathbf{I}_{N_{k,u}} + \sum_{(i,j) \neq (k,u)} \mathbb{E} \left\{ \mathbf{G}_{k,u} \mathbf{\Lambda}_{i,j} \mathbf{G}_{k,u}^H \right\}. \quad (27)$$

Compared to the original transmit covariance optimization problem in (22), the number of the optimization variables in (24) is significantly reduced. In the following, we will develop efficient algorithms to solve the problem in (24).

### B. Iterative Algorithm for DL Power Allocation

Now we focus on the design of the DL power allocation algorithm. We first utilize CCCP to find a local optimum of problem (24). In order to reduce the computational complexity, we then develop a DE based power allocation algorithm.

1) *CCCP Method:* Since  $f_{k,u}^+(\mathbf{\Lambda})$  in (25) and  $f_{k,u}^-(\mathbf{\Lambda})$  in (26) are both concave, the objective in (24) is a difference of concave (d.c.) functions, and the problem is known to be non-deterministic polynomial time hard (NP-hard). For the d.c. problem, it has been shown that the CCCP approach, i.e., a minorization-maximization algorithm, can be an efficient solution [47]. The main idea of CCCP is to transform a non-convex problem to a series of easy-to-handle subproblems [47]. In particular, we replace  $f_{k,u}^-(\mathbf{\Lambda})$  with its first-order Taylor expansion and then solve the subproblem in each CCCP iteration, which further yields the next iteration. Then, the problem in (24) is tackled through solving the following sequence of optimization subproblems iteratively

$$\begin{aligned} \mathbf{\Lambda}^{(\ell+1)} = \arg \max_{\mathbf{\Lambda}} \quad & \sum_{u=1}^U \sum_{k=1}^{K_u} \left\{ f_{k,u}^+(\mathbf{\Lambda}) - \tilde{f}_{k,u}^-(\mathbf{\Lambda}; \mathbf{\Lambda}^{(\ell)}) \right\} \\ \text{s.t.} \quad & \text{constraints in (24),} \end{aligned} \quad (28)$$

where

$$\tilde{f}_{k,u}^-(\mathbf{\Lambda}; \mathbf{\Lambda}^{(\ell)}) = f_{k,u}^-(\mathbf{\Lambda}^{(\ell)}) + \text{tr} \left( (\mathbf{\Delta}_{k,u}^{(\ell)})^T \left( \mathbf{\Lambda}_{k,u} - \mathbf{\Lambda}_{k,u}^{(\ell)} \right) \right). \quad (29)$$

In the  $\ell$ -th iteration,  $\Delta_{k,u}^{(\ell)} = \frac{\partial}{\partial \Lambda_{k,u}} \sum_{i=1}^U \sum_{j=1}^{K_i} f_{i,j}^- (\Lambda^{(\ell)})$  is a diagonal matrix, which can be expressed as

$$\Delta_{k,u}^{(\ell)} = \sum_{(i,j) \neq (k,u)} \sum_{n=1}^{N_{i,j}} \frac{\widehat{\mathbf{R}}_{i,j,n}}{\sigma^2 + \text{tr} \left( \Lambda_{\setminus(i,j)}^{(\ell)} \widehat{\mathbf{R}}_{i,j,n} \right)}, \quad (30)$$

where  $\Lambda_{\setminus(i,j)}^{(\ell)} = \sum_{(p,q) \neq (i,j)} \Lambda_{p,q}^{(\ell)}$ , and  $\widehat{\mathbf{R}}_{i,j,n} = \text{diag} \left\{ [\Omega_{i,j}]_{n,:} \right\}$ . Note that the  $t$ -th diagonal element of  $\Delta_{k,u}^{(\ell)}$  is given by

$$\left[ \Delta_{k,u}^{(\ell)} \right]_{t,t} = \sum_{(i,j) \neq (k,u)} \sum_{n=1}^{N_{i,j}} \frac{[\Omega_{i,j}]_{n,t}}{\sigma^2 + \sum_{(p,q) \neq (i,j)} \sum_{m=1}^{M_{\text{tot}}} \left[ \Lambda_{p,q}^{(\ell)} \right]_{m,m} [\Omega_{i,j}]_{n,m}}. \quad (31)$$

According to [25], the objective value sequence generated by (28) will converge. Note that CCCP is an efficient method to solve the d.c. problem, and the optimization result is a locally optimal solution of the original problem in (24).

2) *DE Method*: Note that it is challenging to derive closed-form expressions of  $f_{k,u}^+ (\Lambda)$  due to the expectation operation. If the Monte-Carlo method is adopted, the optimization can be computationally cumbersome as sample averaging is required. Via utilizing the large dimensional random matrix theory [48], [49], the ergodic rate expression can be well approximated by its DE. In particular, the DE of  $f_{k,u}^+ (\Lambda)$  is given by

$$\overline{f}_{k,u}^+ (\Lambda) = \log \left( \det \left( \mathbf{I}_{M_{\text{tot}}} + \Gamma_{k,u} \Lambda_{k,u} \right) \right) + \log \left( \det \left( \widetilde{\Gamma}_{k,u} + \mathbf{K}_{k,u} (\Lambda) \right) \right) - \text{tr} \left( \mathbf{I}_{N_{k,u}} - \widetilde{\Phi}_{k,u}^{-1} \right), \quad (32)$$

where  $\Gamma_{k,u}$  and  $\widetilde{\Gamma}_{k,u}$  are given by

$$\Gamma_{k,u} = \Pi_{k,u} \left( \widetilde{\Phi}_{k,u}^{-1} \mathbf{K}_{k,u}^{-1} \right) \in \mathbb{C}^{M_{\text{tot}} \times M_{\text{tot}}}, \quad (33)$$

$$\widetilde{\Gamma}_{k,u} = \Xi_{k,u} \left( \Phi_{k,u}^{-1} \Lambda_{k,u} \right) \in \mathbb{C}^{N_{k,u} \times N_{k,u}}, \quad (34)$$

respectively.  $\widetilde{\Phi}_{k,u}$  and  $\Phi_{k,u}$  are obtained by the following iterative equations

$$\widetilde{\Phi}_{k,u} = \mathbf{I}_{N_{k,u}} + \Xi_{k,u} \left( \Phi_{k,u}^{-1} \Lambda_{k,u} \right) \mathbf{K}_{k,u}^{-1}, \quad (35)$$

$$\Phi_{k,u} = \mathbf{I}_{M_{\text{tot}}} + \Pi_{k,u} \left( \widetilde{\Phi}_{k,u}^{-1} \mathbf{K}_{k,u}^{-1} \right) \Lambda_{k,u}. \quad (36)$$

Note that  $\mathbf{\Pi}_{k,u}(\mathbf{Y}) \triangleq \mathbb{E}\{\mathbf{G}_{k,u}^H \mathbf{Y} \mathbf{G}_{k,u}\}$  above is a diagonal matrix-valued function with its  $m$ -th element being

$$[\mathbf{\Pi}_{k,u}(\mathbf{Y})]_{m,m} = \text{tr} \left( \text{diag} \left\{ [\mathbf{\Omega}_{k,u}]_{:,m} \right\} \mathbf{Y} \right). \quad (37)$$

By replacing  $f_{k,u}^+(\mathbf{\Lambda})$  with its DE  $\bar{f}_{k,u}^+(\mathbf{\Lambda})$  in (32) in each iteration, the following series of problems instead of (28) are considered

$$\begin{aligned} \mathbf{\Lambda}^{(\ell+1)} = \arg \max_{\mathbf{\Lambda}} & \sum_{u=1}^U \sum_{k=1}^{K_u} \left\{ \bar{f}_{k,u}^+(\mathbf{\Lambda}) - \tilde{f}_{k,u}^-(\mathbf{\Lambda}; \mathbf{\Lambda}^{(\ell)}) \right\} \\ \text{s.t.} & \text{ constraints in (24)}. \end{aligned} \quad (38)$$

Compared with the Monte-Carlo method that averages over the channel realizations for expectation operation, the DE expression  $\bar{f}_{k,u}^+(\mathbf{\Lambda})$  can be calculated using the statistical CSI, i.e.,  $\mathbf{\Omega}_{k,u}, \forall (k, u)$ , in a few iterations with high accuracy [48]. In addition,  $\bar{f}_{k,u}^+(\mathbf{\Lambda})$  is strictly concave on  $\mathbf{\Lambda}$  [50]. Therefore, each sub-problem in (38) is concave with respect to  $\mathbf{\Lambda}$ , and the resulting solution sequence is still guaranteed to converge.

For notational clarity, we define the DE of the DL network transmission sum-rate in the  $\ell$ -th iteration as

$$\bar{R}^{(\ell)} = \sum_{u=1}^U \sum_{k=1}^{K_u} \left\{ \bar{f}_{k,u}^+(\mathbf{\Lambda}^{(\ell)}) - f_{k,u}^-(\mathbf{\Lambda}^{(\ell)}) \right\}. \quad (39)$$

We use set  $\mathcal{C}_v = \{m | \sum_{v'=1}^{v-1} M_{v'} + 1 \leq m \leq \sum_{v'=1}^v M_{v'}\}$  to represent the indices of the elements in  $\mathbf{\Lambda}_{k,u}$  that are related to BS- $v$ . We denote the  $m$ -th diagonal entries of  $\mathbf{\Gamma}_{k,u}, \tilde{\mathbf{\Gamma}}_{k,u}, \mathbf{\Lambda}_{k,u}, \mathbf{\Delta}_{k,u}$ , and  $\hat{\mathbf{R}}_{i,j,n}$  as  $\gamma_{k,u,m}, \tilde{\gamma}_{k,u,m}, \lambda_{k,u,m}, \delta_{k,u,m}$ , and  $\hat{r}_{i,j,m,n}$ , respectively. For problem (38) in the  $\ell$ -th CCCP iteration, we have the following theorem.

*Theorem 2:* The solution to problem (38) is equivalent to that to the following problem

$$\begin{aligned} \max_{\mathbf{\Lambda}} & \sum_{u=1}^U \sum_{k=1}^{K_u} \left\{ \log \left( \det \left( \mathbf{I}_{M_{\text{tot}}} + \mathbf{\Gamma}_{k,u} \mathbf{\Lambda}_{k,u} \right) \right) + \log \left( \det \left( \tilde{\mathbf{\Gamma}}_{k,u} + \mathbf{K}_{k,u}(\mathbf{\Lambda}) \right) \right) - \text{tr} \left( \mathbf{\Delta}_{k,u}^{(\ell)} \mathbf{\Lambda}_{k,u} \right) \right\} \\ \text{s.t.} & \text{ constraints in (24)}. \end{aligned} \quad (40)$$

For a given BS- $v$ , the  $m$ -th element  $\lambda_{k,u,m}^{(\ell+1)}$  of  $\mathbf{\Lambda}_{k,u}^{(\ell+1)}$ ,  $m \in \mathcal{C}_v$ , can be calculated via solving the

following equations

$$\left\{ \begin{array}{l} \frac{\gamma_{k,u,m}^{(\ell)}}{1+\gamma_{k,u,m}^{(\ell)}\lambda_{k,u,m}^{(\ell+1)}} + \sum_{(i,j)\neq(k,u)} \sum_{n=1}^{N_{i,j}} \frac{\hat{r}_{i,j,m,n}}{\tilde{\gamma}_{i,j,n}^{(\ell)} + \sigma^2 + \text{tr}(\hat{\mathbf{R}}_{i,j,n}\Lambda_{(i,j)}^{(\ell+1)})} = \delta_{k,u,m}^{(\ell)} + \mu_v, \mu_v < \chi_{k,u,m}^{(\ell+1)} - \delta_{k,u,m}^{(\ell)}, \\ \lambda_{k,u,m}^{(\ell+1)} = 0, \quad \mu_v \geq \chi_{k,u,m}^{(\ell+1)} - \delta_{k,u,m}^{(\ell)}. \end{array} \right. \quad (41)$$

The Lagrange multipliers,  $\mu_v, v \in \mathcal{U}$ , satisfy the following KKT conditions

$$\mu_v \left( \text{tr} \left( \sum_{u=1}^U \sum_{k=1}^{K_u} \mathbf{E}_v \Lambda_{k,u} \right) - P_v \right) = 0, \quad \mu_v \geq 0, \quad (42)$$

and the auxiliary variable  $\chi_{k,u,m}^{(\ell+1)}$  is given by

$$\chi_{k,u,m}^{(\ell+1)} = \gamma_{k,u,m}^{(\ell+1)} + \sum_{(i,j)\neq(k,u)} \sum_{n=1}^{N_{i,j}} \frac{\hat{r}_{i,j,m,n}}{\tilde{\gamma}_{i,j,n}^{(\ell+1)} + \sigma^2 + \sum_{(p,q,m') \in \mathcal{S}_{k,u,m,i,j}} \hat{r}_{i,j,m',n} \lambda_{p,q,m'}^{(\ell+1)}}, \quad (43)$$

where  $\mathcal{S}_{k,u,m,i,j}$  is the set given by

$$\mathcal{S}_{k,u,m,i,j} = \{(p, q, m') \mid (p, q) \neq (i, j), (p, q, m') \neq (k, u, m), p_q \in \mathcal{K}, m \in \{1, 2, \dots, M_{\text{tot}}\}\}. \quad (44)$$

*Proof:* Please refer to Appendix B. ■

We detail the developed low-complexity beam domain power allocation algorithm in **Algorithm 1**. Note that to obtain  $\Lambda^{(\ell+1)}$  in Step 12 of **Algorithm 1**, an iterative water-filling **Algorithm 2** is utilized via exploiting Theorem 2, where the auxiliary variables adopted in **Algorithm 2** are defined as

$$\begin{aligned} \rho_{k,u,m}^{(\ell)}(x_{k,u,m}) &= \sum_{(i,j)\neq(k,u)} \sum_{n=1}^{N_{i,j}} \frac{\hat{r}_{i,j,m,n}}{\tilde{\gamma}_{i,j,n}^{(\ell)} + \sigma^2 + \hat{r}_{i,j,m,n}x_{k,u,m} + \sum_{(p,q,m') \in \mathcal{S}_{k,u,m,i,j}} \hat{r}_{i,j,m',n}x_{p,q,m'}} \\ &\quad + \frac{\gamma_{k,u,m}^{(\ell)}}{1 + \gamma_{k,u,m}^{(\ell)}x_{k,u,m}} - \delta_{k,u,m}^{(\ell)} - \mu_v, \quad (45) \\ \rho'_{k,u,m}^{(\ell)}(x_{k,u,m}) &= \sum_{(i,j)\neq(k,u)} \sum_{n=1}^{N_{i,j}} \frac{-\hat{r}_{i,j,m,n}^2}{\left( \tilde{\gamma}_{i,j,n}^{(\ell)} + \sigma^2 + \hat{r}_{i,j,m,n}x_{k,u,m} + \sum_{(p,q,m') \in \mathcal{S}_{k,u,m,i,j}} \hat{r}_{i,j,m',n}x_{p,q,m'} \right)^2} \end{aligned}$$

---

**Algorithm 1** DE based DL Iterative Power Allocation Algorithm
 

---

**Input:** Initial power allocation  $\Lambda^{(0)}$ 

- 1: Initialize iteration index  $\ell = 0$  and calculate  $\bar{R}^{(\ell)}$  as (39).
- 2: **repeat**
- 3:   **for all**  $k_u \in \mathcal{K}$  **do**
- 4:     Initialize  $t = 0$  and  $\tilde{\Phi}_{k,u}^{(t)}$ .
- 5:     **repeat**
- 6:       Calculate  $\tilde{\Phi}_{k,u}^{(t+1)}$  and  $\Phi_{k,u}^{(t+1)}$  by (35) and (36).
- 7:        $t = t + 1$ .
- 8:     **until** convergence of  $\tilde{\Phi}_{k,u}^{(t)}$
- 9:     Calculate  $\Gamma_{k,u}^{(\ell)}$  and  $\tilde{\Gamma}_{k,u}^{(\ell)}$  by (33) and (34).
- 10:    Calculate  $\Delta_{k,u}^{(\ell)}$  based on (30).
- 11:   **end for**
- 12:   Solve (38) to obtain  $\Lambda^{(\ell+1)}$  by **Algorithm 2**.
- 13:   Set  $\ell = \ell + 1$  and calculate  $\bar{R}^{(\ell)}$  by (39).
- 14: **until** convergence of  $\bar{R}^{(\ell)}$

**Output:** Power allocation  $\Lambda$ 


---

$$- \frac{\left(\gamma_{k,u,m}^{(\ell)}\right)^2}{\left(1 + \gamma_{k,u,m}^{(\ell)} x_{k,u,m}\right)^2}, \quad (46)$$

$$\mu_v^{\max} = \max_{k,u,m} \left\{ \gamma_{k,u,m}^{(\ell)} + \sum_{(i,j) \neq (k,u)} \sum_{n=1}^{N_{i,j}} \frac{\hat{r}_{i,j,m,n}}{\tilde{\gamma}_{i,j,n}^{(\ell)} + \sigma^2} - \delta_{k,u,m}^{(\ell)} \right\}, \quad (47)$$

respectively.

*Remark 2:* The solution to (41) has the form of the classical water-filling structure, and the water level depends on the Lagrange multiplier  $\mu_v$ . For our considered multi-UT scenario, solving (41) is challenging because of the summation of the fractional functions. Newton-Raphson method [51] is utilized to find the approximate roots of (41) in Step 11 of **Algorithm 2**. In addition, to find the optimal Lagrange multipliers,  $\mu_v, \forall v \in \mathcal{U}$ , the bisection method is utilized. Note that for the case with a single UT- $(k, u)$ , if the power constrains,  $\text{tr}(\mathbf{E}_v \mathbf{\Lambda}_{k,u}) = P_v, \forall v$ , are considered, the solution can be obtained in closed-form as follows

$$\lambda_{k,u,m}^{(\ell+1)} = \left[ \left( \delta_{k,u,m}^{(\ell)} + \mu_v \right)^{-1} - \left( \gamma_{k,u,m}^{(\ell+1)} \right)^{-1} \right]^+, \quad m \in \mathcal{C}_v, \quad \forall v, \quad (48)$$

where  $\mu_v$  is chosen to satisfy the constraint  $\text{tr}(\mathbf{E}_v \mathbf{\Lambda}_{k,u}) = P_v$ .

---

**Algorithm 2** DL Iterative Water-filling Algorithm
 

---

**Input:** Initial power allocation  $\Lambda^{(\ell)}$  and transmit power  $P_v, \forall v$

- 1: Initialize diagonal matrices  $\bar{\mathbf{X}}_{k,u}^{(0)} = \Lambda_{k,u}^{(\ell)}, \forall (k, u) \in \mathcal{K}$ , threshold  $\epsilon$ , and  $\bar{x}_{k,u,m}$  is the  $m$ -th diagonal entries of  $\bar{\mathbf{X}}_{k,u}$ .
  - 2: **for** all  $v \in \mathcal{U}$  **do**
  - 3:     Set iteration index  $j = 0, \mu_v^{\min,j} = 0$ . Calculate  $\mu_v^{\max,j}$  by (47).
  - 4:     Initialize  $\mu_v^j = (\mu_v^{\min,j} + \mu_v^{\max,j}) / 2$ .
  - 5:     **repeat**
  - 6:         **for** all  $(k, u) \in \mathcal{K}$  **do**
  - 7:             **for**  $m \in \mathcal{C}_v$  **do**
  - 8:                 Set  $w = 0$  and  $x_{k,u,m}^{(j,w)} = \bar{x}_{k,u,m}^{(j)}$ .
  - 9:                 **repeat**
  - 10:                     Calculate  $\rho_{k,u,m}^{(\ell)}(x_{k,u,m}^{(j,w)})$  and  $\rho'_{k,u,m}^{(\ell)}(x_{k,u,m}^{(j,w)})$  as (45) and (46).
  - 11:                     Update  $x_{k,u,m}^{(j,w+1)} = x_{k,u,m}^{(j,w)} - \rho_{k,u,m}^{(\ell)}(x_{k,u,m}^{(j,w)}) / \rho'_{k,u,m}^{(\ell)}(x_{k,u,m}^{(j,w)})$ .
  - 12:                     Set  $w = w + 1$ .
  - 13:                     **until** convergence of  $x_{k,u,m}^{(j,w)}$
  - 14:                     Update  $\bar{x}_{k,u,m}^{(j)} = [x_{k,u,m}^{(j,w)}]^+$ .
  - 15:                 **end for**
  - 16:             **end for**
  - 17:             Calculate  $p_v^{\text{tot}} = \sum_{(k,u) \in \mathcal{K}} \sum_{m \in \mathcal{C}_v} \bar{x}_{k,u,m}^{(j)}$ .
  - 18:             **if**  $p_v^{\text{tot}} \leq P_v$  **then**
  - 19:                 Update  $\mu_v^{\max,j+1} = \mu_v^j$  and  $\mu_v^{\min,j+1} = \mu_v^{\min,j}$ .
  - 20:             **else**
  - 21:                 Update  $\mu_v^{\min,j+1} = \mu_v^j$  and  $\mu_v^{\max,j+1} = \mu_v^{\max,j}$ .
  - 22:             **end if**
  - 23:             Update  $\mu_v^{j+1} = (\mu_v^{\min,j+1} + \mu_v^{\max,j+1}) / 2$  and set  $j = j + 1$ .
  - 24:             **until**  $|p_v^{\text{tot}} - P_v| \leq \epsilon$
  - 25:     **end for**
  - 26: Update  $\Lambda_{k,u}^{(\ell+1)} = \bar{\mathbf{X}}_{k,u}, \forall (k, u) \in \mathcal{K}$ .
- Output:** Power allocation  $\Lambda^{(\ell+1)}$
- 

#### IV. NUMERICAL RESULTS

In this section, numerical results are presented to evaluate the performance of the proposed network massive MIMO transmission over the mmWave/THz bands, where two typical carrier frequencies, 28 GHz and 100 GHz, are adopted. We consider a 120° three-sector cellular model [52], where the cell radius is set to be 100 meters, and the UTs are uniformly distributed in each sector. Table I illustrates the simulation setup. We utilize the mmWave/THz channel model similar to that in [9], [22], where the number of channel clusters is set to 4, and each cluster consists of 20 subpaths. The delay spread and angle spread are set to be 1388.4 ns and 2°, respectively

TABLE I  
SIMULATION SETUP PARAMETERS

Parameter	Value
Carrier frequency	28 GHz, 100 GHz
Sampling interval $T_s$	6.51 ns
Subcarrier spacing	75 kHz
Number of subcarriers $N_{\text{us}}$	2048
CP length $N_{\text{cp}}$	144
Cell radius $R$	100 m, $\forall u$
Number of cells $U$	3
BS array topology	UPA with half-wavelength antenna spacing
Number of BS antennas $M_u^h \times M_u^v$	$32 \times 4$ , $\forall u$
Number of UTs in each sector $K_u$	4, $\forall u$
UT array topology	ULA with half-wavelength antenna spacing
Number of UT antennas $N_{k,u}$	16, 64, $\forall(k, u)$
Noise variance $\sigma^2$	-40 dBm

[22]. In addition, the large-scale fading parameters are summarized in Table II according to [2].

TABLE II  
LARGE-SCALE FADING PARAMETERS

Parameters	Model	LOS	NLOS	outage
Path loss	Eq. (2)	$a^{\text{LOS}} = 61.4$	$a^{\text{NLOS}} = 72.0$	$\zeta_{k,u,v}^{\text{out}} = \infty$ [22]
		$b^{\text{LOS}} = 2$	$b^{\text{NLOS}} = 2.92$	
		$\xi^{\text{LOS}} = 5.8$ dB	$\xi^{\text{NLOS}} = 8.7$ dB	
Channel state	Eq. (1)	$1/a_{\text{out}} = 30.0$ m, $1/a_{\text{los}} = 67.1$ m, $b_{\text{out}} = 5.2$		

We consider the following two approaches as the performance comparison baseline: 1) the **coordinated** transmission approach, where the BSs utilize the statistical CSI of all UTs in the network but only transmit signals to the UTs in its cell [25]; 2) the traditional **single-cell** transmission approach, where the BS in each cell utilizes the statistical CSI of UTs in its cell and transmits signals to the corresponding UTs.

Fig. 1 presents the convergence behavior of **Algorithm 1** under different values of transmit power budgets. The simulation results indicate that our proposed **Algorithm 1** generates a non-decreasing DL network sum-rate sequence and converges fast in typical transmit power budget regions. In particular, the DL network sum-rate can usually converge after only one or two iterations in the case of low transmit power budgets.

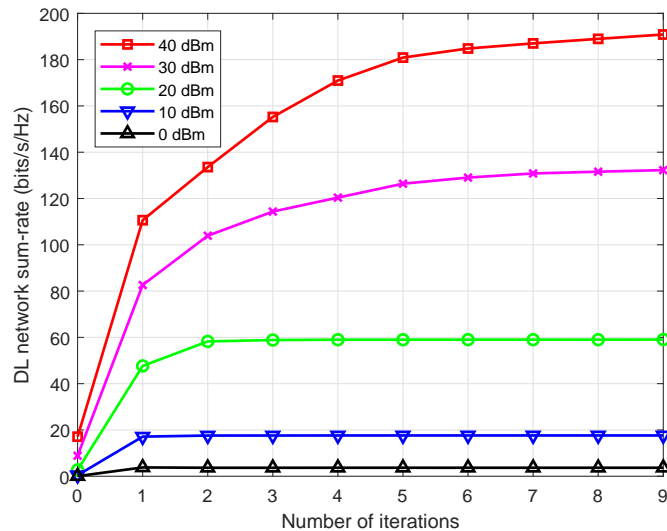


Fig. 1. Convergence behavior of **Algorithm 1**. Results are shown versus the numbers of iterations for different values of transmit power with a carrier frequency of 28 GHz.

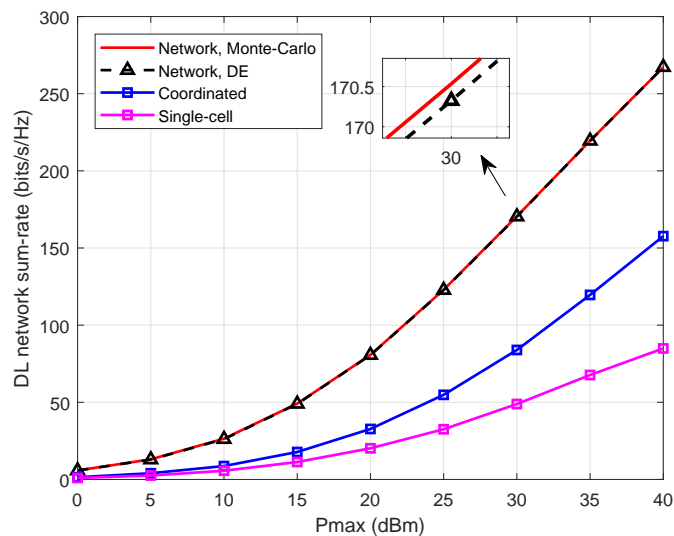


Fig. 2. The DL network sum-rate performance comparison between the proposed network, coordinated, and single-cell transmission approaches with a carrier frequency of 28 GHz. The DE results are also depicted.

Fig. 2 compares the DL network sum-rate performance of the proposed network transmission approach with the baseline ones. We observe that the proposed network transmission approach outperforms the coordinated and single-cell baseline ones, especially at the high power budget regime. Notably, for the case with  $P_{\max} = 40$  dBm, the proposed network transmission approach can provide about 70% performance gains over the coordinated ones. In addition, we can also

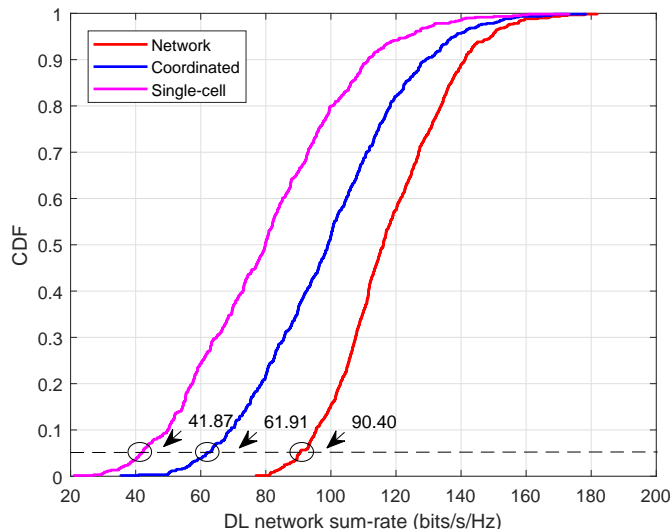


Fig. 3. Cumulative distributive function (CDF) performance of the DL network sum-rate for different approaches with 28 GHz carrier frequency,  $M_u = 16 \times 4, \forall u, N_{k,u} = 8, \forall (k, u) \in \mathcal{K}, P_{\max} = 40$  dBm.

observe that the adopted DE results are almost identical to those obtained from the Monte-Carlo method.

We plot the cumulative distributions of the DL network sum-rate of our proposed approach in Fig. 3. To reduce the simulation complexity, we set  $M_u = 16 \times 4, \forall u, N_{k,u} = 8, \forall (k, u) \in \mathcal{K}$ . The transmit power budget is set to be 40 dBm. Denote the 5% DL sum-rate metric as  $R_{0.05}$ , i.e.,  $\Pr\{R \geq R_{0.05}\} \geq 95\%$ . As can be seen from Fig. 3, the proposed network transmission approach can provide about 116% and 46% performance gains in terms of  $R_{0.05}$  over the traditional single-cell and the coordinated baselines, respectively. The performance gains can be attributed to the following two aspects: 1) when the propagation link between a UT and the BS in its cell is blocked, the BSs of other cells in the network can transmit signals to this UT, which can mitigate the blockage effect, resulting in transmission performance gains; 2) when the transmission link state of a UT and the BS in its cell is good, the BSs in other cells in the network can still transmit signals to this UT. The array gain can further lead to performance gains over the traditional approaches.

Fig. 4 further compares the proposed network transmission approach with the coordinated baseline. Firstly, in order to evaluate the effect of blockage on the two approaches, we fix  $p_{\text{out}}$  of formula (1a) as  $p_{\text{out}} = 0.1$  in Fig. (4a) and  $p_{\text{out}} = 0.5$  in Fig. (4b), respectively. For the case with  $P_{\max} = 40$  dBm, it can be observed that the performance gain of the proposed network

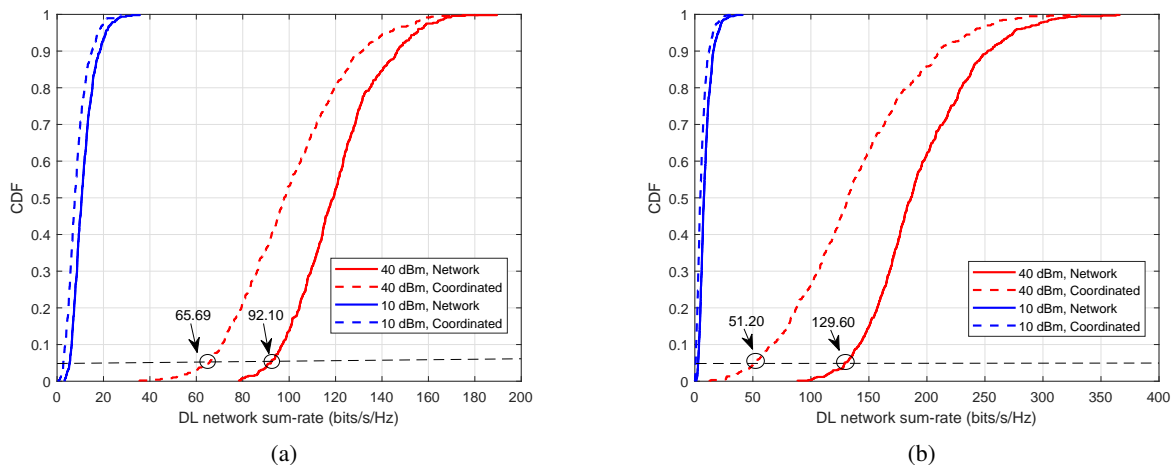


Fig. 4. CDF performance of the DL network sum-rate for the network and coordinated transmission approaches. (a) 28 GHz,  $M_u = 16 \times 4, \forall u, N_{k,u} = 8, \forall (k, u) \in \mathcal{K}, p_{out} = 0.1$ ; (b) 100 GHz,  $M_u = 16 \times 4, \forall u, N_{k,u} = 32, \forall (k, u) \in \mathcal{K}, p_{out} = 0.5$ .

transmission is more significant in the severer THz blockage scenarios. Notably, we can observe the performance gains of  $R_{0.05}$  in Fig. (4a) and in Fig. (4b) are 40.2% and 153.1%, respectively. In addition, the proposed network transmission approach has an average transmission rate gain of 20.1% in Fig. (4a) and 41.2% in Fig. (4b), respectively. With the above observations, we find that the proposed network transmission approach presents significant transmission performance gain over the traditional coordinated one, especially when the channel is severely blocked. Furthermore, we can also observe that in the case of high transmit power budget  $P_{max}$ , the performance gain of the proposed approach is more significant.

Fig. 5 evaluates the performance of our proposed approach under different mobility scenarios. We adopt a tight universal upper bound of the ICI power due to the Doppler effects as in [53], [54]. We compare the DL network sum-rate performance with PBS and the conventional space domain synchronization [42]. The ideal case where channels are static and can be perfectly obtained is presented as the comparison benchmark. We can observe that the PBS scheme outperforms the conventional one, especially in high mobility scenarios, which demonstrates the effectiveness of our proposed transmission approach for mobility enhancement over the mmWave and THz bands.

## V. CONCLUSION

We have investigated network transmission with only the statistical CSI at the BSs to address the challenging issues of mobility enhancement and blockage mitigation in massive MIMO

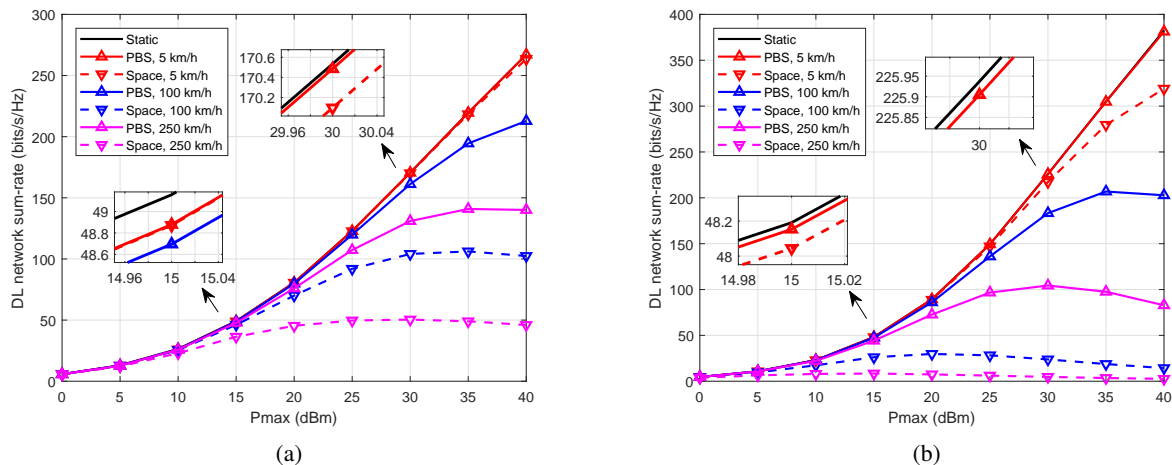


Fig. 5. Comparison of the DL network sum-rate performance with PBS and the conventional space domain synchronization. (a) 28 GHz,  $N_{k,u} = 16, \forall (k, u) \in \mathcal{K}$ ; (b) 100 GHz,  $N_{k,u} = 64, \forall (k, u) \in \mathcal{K}$ .

mmWave/THz communications. Considering the mmWave/THz propagation characteristics, we have proposed to apply the PBS scheme for network massive MIMO to mitigate the channel Doppler and delay dispersions, and established a transmission model accordingly. Our design goal has been successfully transformed into the maximization of the DL network transmission sum-rate. We have shown the optimality of the beam domain transmission, and demonstrated that different BSs can work individually when sending signals to UTs. We have also developed a low-complexity iterative algorithm with guaranteed convergence based on the CCCP and random matrix theory. The KKT conditions have been used to solve the problem in each iteration. We have shown that the solution of the KKT conditions has a classical water-filling structure. As a result, an iterative water-filling power allocation algorithm with guaranteed convergence has been proposed. Numerical results have demonstrated the effectiveness of the proposed transmission approach for alleviating the blockage effects and providing mobility enhancement over the mmWave and THz bands.

## APPENDIX A

### PROOF OF THEOREM 1

From (19) and (20), we can observe that  $\mathbf{K}_{k,u}$  is a diagonal matrix, and the off-diagonal entries of  $\mathbf{Q}_{i,j}, \forall (i, j) \neq (k, u)$ , will not affect the value of  $\mathbf{K}_{k,u}$ . Using a method similar to that in [55], we define a diagonal matrix  $\Upsilon_m \in \mathbb{R}^{M_{\text{tot}} \times M_{\text{tot}}}$  whose diagonal entries are 1 except the

$(m, m)$ -th entry, which is  $-1$ . The off-diagonals in the  $m$ -th row and  $m$ -th column of matrices  $\Upsilon_m \mathbf{Q}_{k,u} \Upsilon_m$  and  $\mathbf{Q}_{k,u}$  have the same absolute values but opposite signs, and the other entries of matrix  $\Upsilon_m \mathbf{Q}_{k,u} \Upsilon_m$  are equal to those of  $\mathbf{Q}_{k,u}$ .

Note that  $\Upsilon_m \mathbf{Q}_{k,u} \Upsilon_m \odot \mathbf{I} = \mathbf{Q}_{k,u} \odot \mathbf{I}$ , we then have

$$\begin{aligned}
R(\mathbf{Q}_{1,1}, \dots, \mathbf{Q}_{K_U, U}) &= \sum_{u=1}^U \sum_{k=1}^{K_u} \mathbb{E} \left\{ \log \left( \det \left( \mathbf{I} + \mathbf{K}_{k,u}^{-1} \mathbf{G}_{k,u} \mathbf{Q}_{k,u} \mathbf{G}_{k,u}^H \right) \right) \right\} \\
&\stackrel{(a)}{=} \sum_{u=1}^U \sum_{k=1}^{K_u} \mathbb{E} \left\{ \log \left( \det \left( \mathbf{I} + \mathbf{K}_{k,u}^{-1} \mathbf{G}_{k,u} \Upsilon_m \mathbf{Q}_{k,u} \Upsilon_m \mathbf{G}_{k,u}^H \right) \right) \right\} \\
&= R(\Upsilon_m \mathbf{Q}_{1,1} \Upsilon_m, \dots, \Upsilon_m \mathbf{Q}_{K_U, U} \Upsilon_m). \tag{49}
\end{aligned}$$

Because of the independence of the columns of  $\mathbf{G}_{k,u}$  and their symmetric distributions, reserving the sign of the  $m$ -th column does not change its distribution. Consequently, (a) is established.

Note that compared to  $\mathbf{Q}_{k,u}$ , the effect of computing  $\frac{1}{2}(\mathbf{Q}_{k,u} + \Upsilon_m \mathbf{Q}_{k,u} \Upsilon_m)$  is to null the off-diagonal entries in the  $m$ -th row and  $m$ -th column of  $\mathbf{Q}_{k,u}$ . Moreover, because of the concavity of  $\log(\det(\cdot))$ , using Jensen's inequality, we have

$$\begin{aligned}
&R\left(\frac{1}{2}(\mathbf{Q}_{1,1} + \Upsilon_m \mathbf{Q}_{1,1} \Upsilon_m), \dots, \frac{1}{2}(\mathbf{Q}_{K_U, U} + \Upsilon_m \mathbf{Q}_{K_U, U} \Upsilon_m)\right) \\
&= \sum_{u=1}^U \sum_{k=1}^{K_u} \mathbb{E} \left\{ \log \left( \det \left( \mathbf{I} + \frac{1}{2} \mathbf{K}_{k,u}^{-1} \mathbf{G}_{k,u} (\mathbf{Q}_{k,u} + \Upsilon_m \mathbf{Q}_{k,u} \Upsilon_m) \mathbf{G}_{k,u}^H \right) \right) \right\} \\
&\geq \frac{1}{2} \sum_{u=1}^U \sum_{k=1}^{K_u} \mathbb{E} \left\{ \log \left( \det \left( \mathbf{I} + \mathbf{K}_{k,u}^{-1} \mathbf{G}_{k,u} \mathbf{Q}_{k,u} \mathbf{G}_{k,u}^H \right) \right) \right\} \\
&\quad + \frac{1}{2} \sum_{u=1}^U \sum_{k=1}^{K_u} \mathbb{E} \left\{ \log \left( \det \left( \mathbf{I} + \mathbf{K}_{k,u}^{-1} \mathbf{G}_{k,u} \Upsilon_m \mathbf{Q}_{k,u} \Upsilon_m \mathbf{G}_{k,u}^H \right) \right) \right\} \\
&= \frac{1}{2} R(\mathbf{Q}_{1,1}, \dots, \mathbf{Q}_{K_U, U}) + \frac{1}{2} R(\Upsilon_m \mathbf{Q}_{1,1} \Upsilon_m, \dots, \Upsilon_m \mathbf{Q}_{K_U, U} \Upsilon_m) \\
&= R(\mathbf{Q}_{1,1}, \dots, \mathbf{Q}_{K_U, U}). \tag{50}
\end{aligned}$$

Thus, we can increase the DL network transmission sum-rate  $R$  by nulling the off-diagonal entries in the  $m$ -th row and  $m$ -th column of  $\mathbf{Q}_{1,1}, \dots, \mathbf{Q}_{K_U, U}$ . Repeating this process for  $m$  from 1 to  $M_{\text{tot}}$ , we draw the conclusion that  $R$  is maximized when  $\mathbf{Q}_{1,1}, \dots, \mathbf{Q}_{K_U, U}$  are all diagonal. This concludes the proof.

APPENDIX B  
PROOF OF THEOREM 2

We define the Lagrangian function of the problem in (38) as follows

$$F = \sum_{u=1}^U \sum_{k=1}^{K_u} \left\{ \bar{f}_{k,u}^+(\mathbf{\Lambda}) - f_{k,u}^-(\mathbf{\Lambda}^{(\ell)}) - \text{tr} \left( \mathbf{\Delta}_{k,u}^{(\ell)} \left( \mathbf{\Lambda}_{k,u} - \mathbf{\Lambda}_{k,u}^{(\ell)} \right) \right) \right\} \\ + \sum_{u=1}^U \sum_{k=1}^{K_u} \text{tr}(\mathbf{\Psi}_{k,u} \mathbf{\Lambda}_{k,u}) - \sum_{v=1}^U \mu_v \left( \text{tr} \sum_{u=1}^U \sum_{k=1}^{K_u} (\mathbf{E}_v \mathbf{\Lambda}_{k,u}) - P_v \right), \quad (51)$$

where the Lagrange multipliers  $\mathbf{\Psi}_{k,u} \succeq \mathbf{0}$  and  $\mu_v \geq 0$  are related to the problem constraints.

The gradient of  $\bar{f}_{k,u}^+(\mathbf{\Lambda})$  with respect to  $\mathbf{\Lambda}_{k,u}$  can be derived from (32) as

$$\frac{\partial}{\partial \mathbf{\Lambda}_{k,u}} \bar{f}_{k,u}^+(\mathbf{\Lambda}) = (\mathbf{I}_{M_{\text{tot}}} + \mathbf{\Gamma}_{k,u} \mathbf{\Lambda}_{k,u})^{-1} \mathbf{\Gamma}_{k,u} \\ + \sum_{m,n} \frac{\partial \bar{f}_{k,u}^+(\mathbf{\Lambda})}{\partial [\mathbf{\Xi}_{k,u}(\mathbf{\Phi}_{k,u}^{-1} \mathbf{\Lambda}_{k,u})]_{m,n}} \frac{\partial [\mathbf{\Xi}_{k,u}(\mathbf{\Phi}_{k,u}^{-1} \mathbf{\Lambda}_{k,u})]_{m,n}}{\partial \mathbf{\Lambda}_{k,u}} \\ + \sum_{m,n} \frac{\partial \bar{f}_{k,u}^+(\mathbf{\Lambda})}{\partial [\mathbf{\Pi}_{k,u}(\mathbf{\tilde{\Phi}}_{k,u}^{-1} \mathbf{K}_{k,u})]_{m,n}} \frac{\partial [\mathbf{\Pi}_{k,u}(\mathbf{\tilde{\Phi}}_{k,u}^{-1} \mathbf{K}_{k,u})]_{m,n}}{\partial \mathbf{\Lambda}_{k,u}}. \quad (52)$$

Following an approach similar to that for proving Theorem 4 in [48], we have

$$\frac{\partial \bar{f}_{k,u}^+(\mathbf{\Lambda})}{\partial [\mathbf{\Xi}_{k,u}(\mathbf{\Phi}_{k,u}^{-1} \mathbf{\Lambda}_{k,u})]_{m,n}} = 0, \quad (53)$$

$$\frac{\partial \bar{f}_{k,u}^+(\mathbf{\Lambda})}{\partial [\mathbf{\Pi}_{k,u}(\mathbf{\tilde{\Phi}}_{k,u}^{-1} (\mathbf{K}_{k,u})^{-1})]_{m,n}} = 0, \quad (54)$$

which further leads to

$$\frac{\partial}{\partial \mathbf{\Lambda}_{k,u}} \bar{f}_{k,u}^+(\mathbf{\Lambda}) = (\mathbf{I}_{M_{\text{tot}}} + \mathbf{\Gamma}_{k,u} \mathbf{\Lambda}_{k,u})^{-1} \mathbf{\Gamma}_{k,u}. \quad (55)$$

In addition, we can obtain the gradient of  $\bar{f}_{k,u}^+(\mathbf{\Lambda})$  over  $\mathbf{\Lambda}_{i,j}$ ,  $\forall (i,j) \neq (k,u)$ , as

$$\frac{\partial}{\partial \mathbf{\Lambda}_{i,j}} \bar{f}_{k,u}^+(\mathbf{\Lambda}) = \sum_{n=1}^{N_{k,u}} \frac{\hat{\mathbf{R}}_{i,j,n}}{\tilde{\gamma}_{i,j,n} + \sigma^2 + \text{tr}(\hat{\mathbf{R}}_{i,j,n} \mathbf{\Lambda}_{\setminus(i,j)}}. \quad (56)$$

Then, from (55) and (56), we have

$$\begin{aligned} \frac{\partial}{\partial \Lambda_{a,b}} \sum_{u=1}^U \sum_{k=1}^{K_u} \bar{f}_{k,u}^+(\Lambda) &= (\mathbf{I}_{M_{\text{tot}}} + \Gamma_{a,b} \Lambda_{a,b})^{-1} \Gamma_{a,b} \\ &+ \sum_{(k,u) \neq (a,b)} \sum_{n=1}^{N_{k,u}} \frac{\widehat{\mathbf{R}}_{k,u,n}}{\tilde{\gamma}_{k,u,n} + \sigma^2 + \text{tr}(\widehat{\mathbf{R}}_{k,u,n} \Lambda_{\setminus(k,u)}}). \end{aligned} \quad (57)$$

Owing to the concavity of  $\bar{f}_{k,u}^+(\Lambda)$  over  $\Lambda$ , the KKT conditions of (38) are

$$\frac{\partial F}{\partial \Lambda_{k,u}^{(\ell+1)}} = \mathbf{0}, \quad (58a)$$

$$\text{tr}(\Psi_{k,u}^{(\ell+1)} \Lambda_{k,u}^{(\ell+1)}) = 0, \quad \Psi_{k,u}^{(\ell+1)} \succeq \mathbf{0}, \quad \Lambda_{k,u}^{(\ell+1)} \succeq \mathbf{0}, \quad (58b)$$

$$\mu_v \left( \text{tr} \left( \sum_{u=1}^U \sum_{k=1}^{K_u} (\mathbf{E}_v \Lambda_{k,u}) - P_v \right) \right) = 0, \quad \mu_v \geq 0, \quad \forall (k,u) \in \mathcal{K}. \quad (58c)$$

Utilizing the concavity of problem (38), we can get the optimal solution  $\Lambda_{k,u}^{(\ell+1)}$  by solving the corresponding KKT conditions. We reformulate the first KKT condition in (58a) as

$$\begin{aligned} \frac{\partial F}{\partial \Lambda_{k,u}^{(\ell+1)}} &= \left( \mathbf{I}_{M_{\text{tot}}} + \Gamma_{k,u}^{(\ell+1)} \Lambda_{k,u}^{(\ell+1)} \right)^{-1} \Gamma_{k,u}^{(\ell+1)} - \Delta_{k,u}^{(\ell)} + \Psi_{k,u}^{(\ell+1)} - \mu_v^{(\ell)} \mathbf{E}_v \\ &+ \sum_{(i,j) \neq (k,u)} \sum_{n=1}^{N_{i,j}} \frac{\widehat{\mathbf{R}}_{i,j,n}}{\tilde{\gamma}_{i,j,n}^{(\ell+1)} + 1 + \text{tr}(\widehat{\mathbf{R}}_{i,j,n} \Lambda_{\setminus(i,j)}^{(\ell+1)})} = \mathbf{0}. \end{aligned} \quad (59)$$

It can be found that the KKT conditions in (58) equal to those of the following problem

$$\begin{aligned} \arg \max_{\Lambda} \quad & \sum_{u=1}^U \sum_{k=1}^{K_u} \left\{ \log(\det(\mathbf{I}_{M_{\text{tot}}} + \Gamma_{k,u} \Lambda_{k,u})) + \log(\det(\tilde{\Gamma}_{k,u} + \mathbf{K}_{k,u}(\Lambda))) \right. \\ & \left. - \text{tr}(\Delta_{k,u}^{(\ell)} \Lambda_{k,u}) \right\} \\ \text{s.t.} \quad & \text{tr} \left( \sum_{u=1}^U \sum_{k=1}^{K_u} (\mathbf{E}_v \Lambda_{k,u}) \right) \leq P_v, \quad \forall v \in \mathcal{U}, \\ & \Lambda_{k,u} \succeq \mathbf{0}, \quad \Lambda_{k,u} \text{ diagonal}, \quad \forall (k,u) \in \mathcal{K}. \end{aligned} \quad (60)$$

Solving the corresponding KKT conditions, we have

$$\left\{ \begin{array}{l} \frac{\gamma_{k,u,m}^{(\ell)}}{1+\gamma_{k,u,m}^{(\ell)}\lambda_{k,u,m}^{(\ell+1)}} + \sum_{(i,j)\neq(k,u)} \sum_{n=1}^{N_{i,j}} \frac{\hat{r}_{i,j,m,n}}{\tilde{\gamma}_{i,j,n}^{(\ell)} + \sigma^2 + \text{tr}(\hat{\mathbf{R}}_{i,j,n}\Lambda_{(i,j)}^{(\ell+1)})} = \delta_{k,u,m}^{(\ell)} + \mu_v, \mu_v < \chi_{k,u,m}^{(\ell+1)} - \delta_{k,u,m}^{(\ell)}, \\ \lambda_{k,u,m}^{(\ell+1)} = 0, \end{array} \right. \quad \mu_v \geq \chi_{k,u,m}^{(\ell+1)} - \delta_{k,u,m}^{(\ell)}, \quad (61)$$

where the auxiliary variable  $\chi_{k,u,m}^{(\ell+1)}$  is expressed as

$$\chi_{k,u,m}^{(\ell+1)} = \gamma_{k,u,m}^{(\ell+1)} + \sum_{(i,j)\neq(k,u)} \sum_{n=1}^{N_{i,j}} \frac{\hat{r}_{i,j,m,n}}{\tilde{\gamma}_{i,j,n}^{(\ell+1)} + \sigma^2 + \sum_{(p,q,m')\in\mathcal{S}_{k,u,m,i,j}} \hat{r}_{i,j,m',n}\lambda_{p,q,m'}^{(\ell+1)}}. \quad (62)$$

This concludes the proof.

## REFERENCES

- [1] X. Chen, L. You, X. H. Song, F. Jiang, W. J. Wang, X. Q. Gao, and G. Fettweis, "Network massive MIMO transmission over millimeter-wave bands," in *Proc. IEEE ICC*, Dublin, Ireland, 2020, pp. 1–6.
- [2] T. S. Rappaport, S. Sun, R. Mayzus, H. Zhao, Y. Azar, K. Wang, G. N. Wong, J. K. Schulz, M. K. Samimi, and F. Gutierrez, "Millimeter wave mobile communications for 5G cellular: It will work!" *IEEE Access*, vol. 1, pp. 335–349, May 2013.
- [3] M. Xiao, S. Mumtaz, Y. Huang, L. Dai, Y. Li, M. Matthaiou, G. K. Karagiannidis, E. Björnson, K. Yang, C.-L. I, and A. Ghosh, "Millimeter wave communications for future mobile networks," *IEEE J. Sel. Areas Commun.*, vol. 35, no. 9, pp. 1909–1935, Sep. 2017.
- [4] T. S. Rappaport, Y. Xing, O. Kanhere, S. Ju, A. Madanayake, S. Mandal, A. Alkhateeb, and G. C. Trichopoulos, "Wireless communications and applications above 100 GHz: Opportunities and challenges for 6G and beyond," *IEEE Access*, vol. 7, pp. 78 729–78 757, 2019.
- [5] T. L. Marzetta, "Noncooperative cellular wireless with unlimited numbers of base station antennas," *IEEE Trans. Wireless Commun.*, vol. 9, no. 11, pp. 3590–3600, Nov. 2010.
- [6] J. Zhang, E. Björnson, M. Matthaiou, D. W. K. Ng, H. Yang, and D. J. Love, "Prospective multiple antenna technologies for beyond 5G," *arXiv preprint arXiv: 1910.00092v3*, 2020.
- [7] A. L. Swindlehurst, E. Ayanoglu, P. Heydari, and F. Capolino, "Millimeter-wave massive MIMO: The next wireless revolution?" *IEEE Commun. Mag.*, vol. 52, no. 9, pp. 56–62, Sep. 2014.
- [8] J. Huang, C. Wang, R. Feng, J. Sun, W. Zhang, and Y. Yang, "Multi-frequency mmWave massive MIMO channel measurements and characterization for 5G wireless communication systems," *IEEE J. Sel. Areas Commun.*, vol. 35, no. 7, pp. 1591–1605, Jul. 2017.
- [9] L. You, X. Q. Gao, G. Y. Li, X.-G. Xia, and N. Ma, "BDMA for millimeter-wave/Terahertz massive MIMO transmission with per-beam synchronization," *IEEE J. Sel. Areas Commun.*, vol. 35, no. 7, pp. 1550–1563, Jul. 2017.
- [10] B. Wang, F. Gao, S. Jin, H. Lin, and G. Y. Li, "Spatial- and frequency-wideband effects in millimeter-wave massive MIMO systems," *IEEE Trans. Signal Process.*, vol. 66, no. 13, pp. 3393–3406, Jul. 2018.
- [11] B. Ai, K. Guan, R. He, J. Li, G. Li, D. He, Z. Zhong, and K. M. S. Huq, "On indoor millimeter wave massive MIMO channels: Measurement and simulation," *IEEE J. Sel. Areas Commun.*, vol. 35, no. 7, pp. 1678–1690, Jul. 2017.

- [12] X. Gao, L. Dai, Y. Zhang, T. Xie, X. Dai, and Z. Wang, "Fast channel tracking for Terahertz beamspace massive MIMO systems," *IEEE Trans. Veh. Technol.*, vol. 66, no. 7, pp. 5689–5696, Jul. 2017.
- [13] V. Petrov, M. Komarov, D. Moltchanov, J. M. Jornet, and Y. Koucheryavy, "Interference and SINR in millimeter wave and Terahertz communication systems with blocking and directional antennas," *IEEE Trans. Wireless Commun.*, vol. 16, no. 3, pp. 1791–1808, Mar. 2017.
- [14] T. Bai and R. W. Heath, "Coverage and rate analysis for millimeter-wave cellular networks," *IEEE Trans. Wireless Commun.*, vol. 14, no. 2, pp. 1100–1114, Feb. 2015.
- [15] J. G. Andrews, T. Bai, M. N. Kulkarni, A. Alkhateeb, A. K. Gupta, and R. W. Heath, Jr., "Modeling and analyzing millimeter wave cellular systems," *IEEE Trans. Commun.*, vol. 65, no. 1, pp. 403–430, Jan. 2017.
- [16] Y. Azar, G. N. Wong, K. Wang, R. Mayzus, J. K. Schulz, H. Zhao, F. Gutierrez, D. Hwang, and T. S. Rappaport, "28 GHz propagation measurements for outdoor cellular communications using steerable beam antennas in New York City," in *Proc. IEEE ICC*, Budapest, Hungary, 2013, pp. 5143–5147.
- [17] M. Samimi, K. Wang, Y. Azar, G. N. Wong, R. Mayzus, H. Zhao, J. K. Schulz, S. Sun, F. Gutierrez, and T. S. Rappaport, "28 GHz angle of arrival and angle of departure analysis for outdoor cellular communications using steerable beam antennas in New York City," in *Proc. IEEE VTC*, Dresden, Germany, 2013, pp. 1–6.
- [18] C. Han, A. O. Bicen, and I. F. Akyildiz, "Multi-ray channel modeling and wideband characterization for wireless communications in the Terahertz band," *IEEE Trans. Wireless Commun.*, vol. 14, no. 5, pp. 2402–2412, May 2015.
- [19] R. He, B. Ai, G. L. Stüber, G. Wang, and Z. Zhong, "Geometrical-based modeling for millimeter-wave MIMO mobile-to-mobile channels," *IEEE Trans. Veh. Technol.*, vol. 67, no. 4, pp. 2848–2863, Apr. 2018.
- [20] C. Huang, A. F. Molisch, Y.-A. Geng, R. He, B. Ai, and Z. Zhong, "Trajectory-joint clustering algorithm for time-varying channel modeling," *IEEE Trans. Veh. Technol.*, vol. 69, no. 1, pp. 1041–1045, Jan. 2020.
- [21] R. He, C. Schneider, B. Ai, G. Wang, D. Dupleich, R. Thomä, M. Boban, J. Luo, Z. Zhong, and Y. Zhang, "Propagation channels of 5G millimeter wave vehicle-to-vehicle communications: Recent advances and future challenges," *IEEE Veh. Technol. Mag.*, vol. 15, no. 1, pp. 16–26, Jan. 2020.
- [22] M. R. Akdeniz, Y. Liu, M. K. Samimi, S. Sun, S. Rangan, T. S. Rappaport, and E. Erkip, "Millimeter wave channel modeling and cellular capacity evaluation," *IEEE J. Sel. Areas Commun.*, vol. 32, no. 6, pp. 1164–1179, Jun. 2014.
- [23] V. Va, J. Choi, and R. W. Heath, "The impact of beamwidth on temporal channel variation in vehicular channels and its implications," *IEEE Trans. Veh. Technol.*, vol. 66, no. 6, pp. 5014–5029, Jun. 2017.
- [24] Q. Zhang, S. Jin, M. McKay, D. Morales-Jimenez, and H. Zhu, "Power allocation schemes for multicell Massive MIMO systems," *IEEE Trans. Wireless Commun.*, vol. 14, no. 11, pp. 5941–5955, Nov. 2015.
- [25] C. Sun, X. Q. Gao, and Z. Ding, "BDMA in multicell massive MIMO communications: Power allocation algorithms," *IEEE Trans. Signal Process.*, vol. 65, no. 11, pp. 2962–2974, Jun. 2017.
- [26] H. Q. Ngo, A. Ashikhmin, H. Yang, E. G. Larsson, and T. L. Marzetta, "Cell-free massive MIMO versus small cells," *IEEE Trans. Wireless Commun.*, vol. 16, no. 3, pp. 1834–1850, Mar. 2017.
- [27] Z. Xiang, M. Tao, and X. Wang, "Coordinated multicast beamforming in multicell networks," *IEEE J. Sel. Areas Commun.*, vol. 32, no. 6, pp. 1180–1193, Jun. 2014.
- [28] O. Tervo, H. Pennanen, D. Christopoulos, S. Chatzinotas, and B. Ottersten, "Distributed optimization for coordinated beamforming in multicell multigroup multicast systems: Power minimization and SINR balancing," *IEEE Trans. Signal Process.*, vol. 66, no. 1, pp. 171–185, Jan. 2018.
- [29] M. N. Kulkarni, A. Ghosh, and J. G. Andrews, "A comparison of MIMO techniques in downlink millimeter wave cellular networks with hybrid beamforming," *IEEE Trans. Commun.*, vol. 64, no. 5, pp. 1952–1967, May 2016.

- [30] S. He, Y. Huang, S. Jin, and L. Yang, "Energy efficient coordinated beamforming design in multi-cell multicast networks," *IEEE Commun. Lett.*, vol. 19, no. 6, pp. 985–988, Jun. 2015.
- [31] J. Choi, D. J. Love, and P. Bidigare, "Downlink training techniques for FDD massive MIMO systems: Open-loop and closed-loop training with memory," *IEEE J. Sel. Topics Signal Process.*, vol. 8, no. 5, pp. 802–814, Oct. 2014.
- [32] R. He, B. Ai, G. Wang, K. Guan, Z. Zhong, A. F. Molisch, C. Briso-Rodriguez, and C. P. Oestges, "High-speed railway communications: From GSM-R to LTE-R," *IEEE Veh. Technol. Mag.*, vol. 11, no. 3, pp. 49–58, Sep. 2016.
- [33] J. Wang, S. Jin, X. Q. Gao, K.-K. Wong, and E. Au, "Statistical eigenmode-based SDMA for two-user downlink," *IEEE Trans. Signal Process.*, vol. 60, no. 10, pp. 5371–5383, Oct. 2012.
- [34] M. Barzegar Khalilsarai, S. Haghghatshoar, X. Yi, and G. Caire, "FDD massive MIMO via UL/DL channel covariance extrapolation and active channel sparsification," *IEEE Trans. Wireless Commun.*, vol. 18, no. 1, pp. 121–135, Jan. 2018.
- [35] L. You, X. Q. Gao, A. L. Swindlehurst, and W. Zhong, "Channel acquisition for massive MIMO-OFDM with adjustable phase shift pilots," *IEEE Trans. Signal Process.*, vol. 64, no. 6, pp. 1461–1476, Mar. 2016.
- [36] L. You, K.-X. Li, J. Wang, X. Q. Gao, X.-G. Xia, and B. Ottersten, "Massive MIMO transmission for LEO satellite communications," *arXiv preprint arXiv:2002.08148*, 2020.
- [37] H. Huh, A. M. Tulino, and G. Caire, "Network MIMO with linear zero-forcing beamforming: Large system analysis, impact of channel estimation, and reduced-complexity scheduling," *IEEE Trans. Inf. Theory*, vol. 58, no. 5, pp. 2911–2934, May 2012.
- [38] A. S. Cacciapuoti, R. Subramanian, M. Caleffi, and K. R. Chowdhury, "Software-defined network controlled switching between millimeter wave and Terahertz small cells," *arXiv preprint arXiv:1702.02775*, 2017.
- [39] L. You, X. Q. Gao, X.-G. Xia, N. Ma, and Y. Peng, "Pilot reuse for massive MIMO transmission over spatially correlated Rayleigh fading channels," *IEEE Trans. Wireless Commun.*, vol. 14, no. 6, pp. 3352–3366, Jun. 2015.
- [40] Y. Zeng and R. Zhang, "Millimeter wave MIMO with lens antenna array: A new path division multiplexing paradigm," *IEEE Trans. Commun.*, vol. 64, no. 4, pp. 1557–1571, Apr. 2016.
- [41] T. Hwang, C. Yang, G. Wu, S. Li, and G. Y. Li, "OFDM and its wireless applications: A survey," *IEEE Trans. Veh. Technol.*, vol. 58, no. 4, pp. 1673–1694, May 2009.
- [42] M. Morelli, C.-C. J. Kuo, and M.-O. Pun, "Synchronization techniques for orthogonal frequency division multiple access (OFDMA): A tutorial review," *Proc. IEEE*, vol. 95, no. 7, pp. 1394–1427, Jul. 2007.
- [43] D. Tse and P. Viswanath, *Fundamentals of Wireless Communication*. New York, NY, USA: Cambridge Univ. Press, 2005.
- [44] C. Sun, X. Q. Gao, S. Jin, M. Matthaiou, Z. Ding, and C. Xiao, "Beam division multiple access transmission for massive MIMO communications," *IEEE Trans. Commun.*, vol. 63, no. 6, pp. 2170–2184, Jun. 2015.
- [45] B. Hassibi and B. M. Hochwald, "How much training is needed in multiple-antenna wireless links?" *IEEE Trans. Inf. Theory*, vol. 49, no. 4, pp. 951–963, Apr. 2003.
- [46] A.-A. Lu, X. Q. Gao, W. Zhong, C. Xiao, and X. Meng, "Robust transmission for massive MIMO downlink with imperfect CSI," *IEEE Trans. Commun.*, vol. 67, no. 8, pp. 5362–5376, Aug. 2019.
- [47] Y. Sun, P. Babu, and D. P. Palomar, "Majorization-minimization algorithms in signal processing, communications, and machine learning," *IEEE Trans. Signal Process.*, vol. 65, no. 3, pp. 794–816, Feb. 2017.
- [48] A.-A. Lu, X. Q. Gao, and C. Xiao, "Free deterministic equivalents for the analysis of MIMO multiple access channel," *IEEE Trans. Inf. Theory*, vol. 62, no. 8, pp. 4604–4629, Aug. 2016.
- [49] R. Couillet and M. Debbah, *Random Matrix Methods for Wireless Communications*. New York, NY, USA: Cambridge Univ. Press, 2011.
- [50] J. Dumont, S. Lasaulce, S. Lasaulce, P. Loubaton, and J. Najim, "On the capacity achieving covariance matrix for Rician MIMO channels: An asymptotic approach," *IEEE Trans. Inf. Theory*, vol. 56, no. 3, pp. 1048–1069, Mar. 2010.

- [51] T. H. Cormen, C. E. Leiserson, R. L. Rivest, and C. Stein, *Introduction to Algorithms*, 3rd ed. Cambridge, MA, USA: MIT press, 2009.
- [52] H. Huang, C. B. Papadias, and S. Venkatesan, *MIMO Communication for Cellular Networks*. New York, NY, USA: Springer, 2012.
- [53] Y. Li and L. J. Cimini, "Bounds on the interchannel interference of OFDM in time-varying impairments," *IEEE Trans. Commun.*, vol. 49, no. 3, pp. 401–404, Mar. 2001.
- [54] A. Stamoulis, S. N. Diggavi, and N. Al-Dhahir, "Intercarrier interference in MIMO OFDM," *IEEE Trans. Signal Process.*, vol. 50, no. 10, pp. 2451–2464, Oct. 2002.
- [55] L. You, J. Xiong, X. Yi, J. Wang, W. Wang, and X. Q. Gao, "Energy efficiency optimization for downlink massive MIMO with statistical CSIT," *IEEE Trans. Wireless Commun.*, vol. 19, no. 4, pp. 2684–2698, Apr. 2020.